ATRIAS: Design and Validation of a Tether-free 3D-capable Spring-Mass Bipedal Robot

Christian Hubicki[*], Jesse Grimes[*], Mikhail Jones[*], Daniel Renjewski[†], Alexander Spröwitz[‡], Andy Abate[*] and Jonathan Hurst[*§]

Abstract

ATRIAS is a human-scale 3D-capable bipedal robot designed to mechanically embody the *spring-mass* model for dynamic walking and running. To help bring the extensive work on this theoretical model further into practice, we present the design and validation of a spring-mass robot which can operate in real-world settings (i.e., off-tether and without planarizing restraints). We outline the mechanisms and design choices necessary to meet these specifications, particularly ATRIAS' four-bar series-elastic leg design. We experimentally demonstrate the following robot capabilities, which are characteristics of the target model. 1) We present the robot's physical capability for both grounded and aerial gaits, including planar walking and sustained hopping, while being more efficient than similarly gait-versatile bipeds. 2) The robot can be controlled by enforcing quantities derived from the simpler spring-mass model, such as leg angles and leg forces. 3) ATRIAS replicates the center-of-mass dynamics of human hopping and (novelly) walking, a key spring-mass model feature. Lastly, we present dynamically stable stepping in 3D without external support, demonstrating that this theoretical model has practical potential for real-world locomotion.

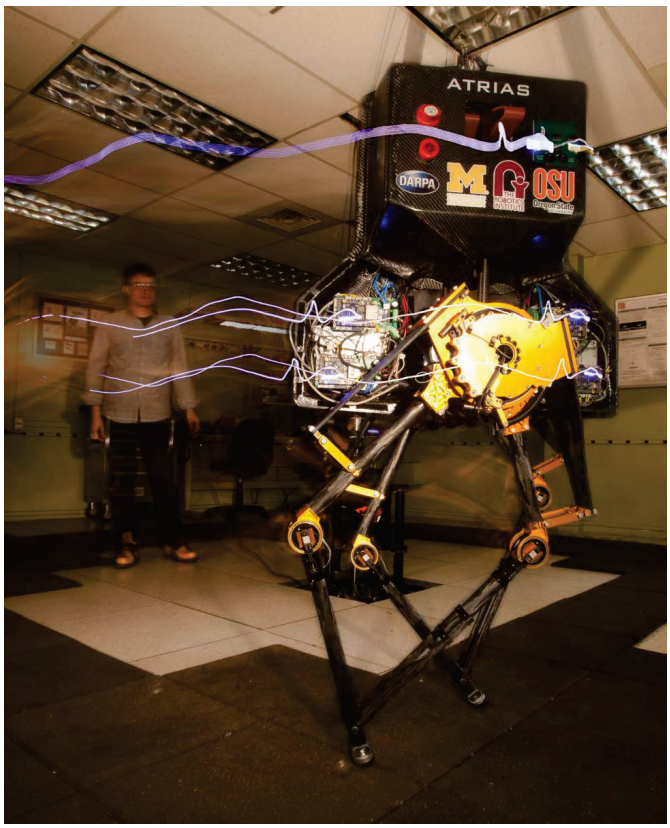

Figure 1: ATRIAS (**A**ssume **T**he **R**obot **I**s **A** **S**phere) is a highly dynamic bipedal robot whose passive dynamics are designed to approximate an agile and efficient reduced-order math model: the *spring-mass model*. Standing 171 cm (5'7") tall and 62 kg (137 lb) with batteries, the human-scale biped is designed to both walk and run, and has the actuation, on-board power, real-time control, and wireless communication necessary to trek untethered through real environments. At present, there are three ATRIAS bipeds in circulation functioning as common research platforms.

1 Introduction

ATRIAS (Figure 1) is a human-scale 3D-capable bipedal robot designed to mechanically embody a

[*]Dynamic Robotics Laboratory, School of Mechanical, Industrial and Manufacturing Engineering, Oregon State University, USA.

[†]Robotics and Embedded Systems Group, Technische Universität München, Germany

[‡]Physical Intelligence Department, Max Planck Institute for Intelligent Systems, Stuttgart, Germany

[§]Corresponding author. Jonathan Hurst can be contacted at `jonathan.hurst@oregonstate.edu`.

far simpler set of dynamics, the *spring-mass model*. The bipedal spring-mass model is a unifying math model that reproduces dynamics for walking and running as seen in animal gaits. We aim to physically reproduce the dynamics of bipedal spring-mass locomotion, specifically characterized by **1)** running/hopping with "single-humped" ground reaction forces, and novelly **2)** walking with "double-humped" ground-reaction forces (Geyer et al. 2006) (Figure 2). Our approach is to design the passive dynamics of ATRIAS (**A**ssume **T**he **R**obot **I**s **A** **S**phere) such that the machine's dynamics naturally respond as if it were an ideal spring mass model, which we abbreviate a "spring-mass robot". By targeting spring-mass dynamics by design, ATRIAS demonstrates that this locomotion theory can be rendered on a practical machine which is 3D-capable (i.e. it requires no power tether or planarizing restraint). We present the design of ATRIAS and experimentally demonstrate the advantages of this design approach, which we categorize: *1) engineering, 2) control synthesis, 3) and biomechanical relevance.*

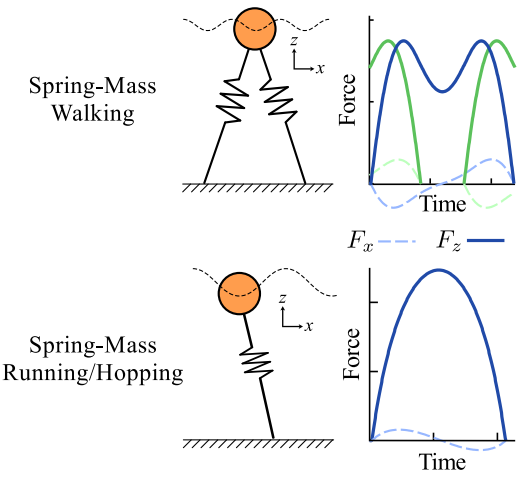

Figure 2: Spring-mass walking and running, as described in (Geyer et al. 2006), which unifies the dynamics of animal walking and running with a single math model. These are the characteristic dynamics of spring-mass gaits, as defined by ground reaction forces: a "double-humped" profile for walking and a "single-humped" profile for running and hopping.

This spring-mass approach has the potential to ameliorate some of the long-standing *engineering* problems in bipedal robotics: particularly, that robots are either too energy consuming or overly specialized to a particular gait. We posit that robots are often held back by inherent dynamical limits which are imposed by their mechanical design. While humanoid robots have long been among the most motion-versatile bipeds, with robots like ASIMO able to walk, run, and hop (Hirose and Ogawa 2007), their design approach does have drawbacks. Many humanoid robots have stiff connections at every joint between their motor rotors, gear trains, and the ground. This means that all positive and negative work in each gait cycle must flow through actuators and transmissions, creating inefficiencies. In contrast, passive dynamic walkers with very limited actuation are paragons of energy economy (Collins et al. 2005), but are too restricted to particular walking speeds, gaits, and motions to be versatile in application. No controller, no matter how clever, can achieve ambitious agility and economy goals if the hardware is too encumbering. As such, ATRIAS aims to find an effective blend of passive dynamics and controlled actuation to achieve locomotion that is both efficient and versatile.

Bipedal robots are also challenging from a *control synthesis* standpoint, in part due to their inherent nonlinearities, hybrid dynamics, numerous degrees of freedom, and occasional underactuation. This approach of building ATRIAS to embody an ideal model provides a reduced-order structure for exploring the control of the complex full-order machine. Further, the spring-mass model has been widely studied in the dynamics and control literature. The results include self-stabilizing techniques (Seyfarth and Geyer 2002), step-planning methods (Piovan and Byl 2013), and dynamic gait speed changes (Ernst et al. 2012). As such, ATRIAS has the potential to be controlled by implementing the same policies, or structurally similar policies (Rezazadeh et al. 2015; Martin et al. 2015), as those developed in the literature.

This design approach also offers an opportunity for achieving locomotion with greater *biomechanical relevance*. The spring-mass model was first introduced in the context of legged locomotion as a biomechanical descriptor, particularly of the center-of-mass running and hopping dynamics in humans (Blickhan 1989). In the decades since, this spring-leg concept has become cemented in the biomechanics community to the point that it is common practice to report "leg stiffness" as a standard quantity in animal locomotion dynamics (Lee et al. 2014). Notably, the spring-mass model has been suggested as a means of unifying running dynamics with walking

(Geyer et al. 2006). We present the ATRIAS robot as the first machine to demonstrate and report these biological walking dynamics.

In overview, we present this case in the following stages. For background, Section 2 catalogs the successes and limitations of bipedal robots and spring-legged robot designs to date, and describes the spring-mass model (ATRIAS' target math model). Section 3 outlines the design features which were key to approximating the spring-mass model, their design impact, and our solutions to constructing a 3D-capable spring-mass biped. Section 4 reports a number of hardware experiments which validate that ATRIAS functions as a spring-mass robot. These passive-dynamic experiments also demonstrate that dropping, pushing, or throwing ATRIAS yielded 3-5 passive hops or 18 passive walking steps before halting[1].

We further demonstrate the capacity of ATRIAS (Figure 3e), and its monopod predecessor (Figure 3d), to execute a variety of dynamic maneuvers when actuation is unleashed: hopping on one leg (a precursor to running), and reflexively recovering from a hop into an unexpected 16.5-cm-deep gravel pit. Particularly, we report walking with human-like center-of-mass dynamics (as measured by ground-reaction forces), which we believe is a novel observation of a walking machine. We measure the economy of our tested walking gait, reporting an electrical cost of transport of 1.13, less than a third the energy cost estimated for some humanoid robots (e.g. ASIMO) (Collins et al. 2005). We also demonstrate its mechanical capability of practical 3D locomotion by showing ATRIAS march in place without planar restraints. Section 5 surveys future work with ATRIAS, particularly in terms of design, control, and biological investigations. In summary, Section 6, we take inventory of ATRIAS' capabilities and assess spring-mass robot design as an approach to enabling agile legged robots that are ready for the real world.

2 Background

The concept of legged locomotion is inspired by nature, but engineered systems, especially bipedal robots, often do not go beyond the stage of morphological biomimetics. Bipedal robots, for example, are frequently built with joints, actuation, and link lengths approximating human morphology, but infrequently approximate biological dynamics. The challenges of keeping balance, managing the dynamic interaction with the environment and adapting trajectories according to terrain changes are addressed in a number of ways.

In varying combinations, existing bipedal robots have exhibited versatile behaviors, been off-tether capable, tackled the challenge of human-scale implementation, and even approximated dynamical model-based behavior like spring-mass running. With ATRIAS, we draw from this array of ideas to achieve spring-mass walking and hopping on a 3D-capable machine that can operate off tether. We outline some key approaches to designing bipedal machines, the robots that emerged as a consequence, and argue why spring-mass model dynamics are a worthwhile design target for achieving a variety of efficient bipedal gaits.

2.1 Fully-Actuated Humanoids

Fully articulated humanoid robots have been the most practical and publicly visible representatives of bipedal locomotion. Notable examples such as Honda's ASIMO (Hirose and Ogawa 2007), AIST's HRP series (Kaneko et al. 2011), KAIST's HUBO (Park et al. 2007) are electromechanically driven, fully actuated machines capable of versatile, autonomous motion carrying their energy source. These high-DOF robots address the challenge of bipedal balance by careful regulation of their zero-moment point (ZMP) (Vukobratović and Borovac 2004). The ZMP framework has been a hallmark of humanoid control for decades thanks to its mathematical tractability.

However, one consequence of ensuring controllability of the ZMP is that it calls for actuators and stiff mechanical connections at every joint. In such gear-driven robot designs without mechanical compliance (as is typically the case with humanoids), there are significant rotor inertias that inherently limit the joint accelerations. We argue this prevents these humanoids from exhibiting the bouncy, highly dynamic locomotion mastered by animals. Bipeds with high leg stiffness also cannot absorb a significant amount of the energy from impacts and must mitigate damage by slowing down the impact velocity (limiting potential dynamic gaits). With full actuation, every joint motion must be accompanied

[1] Tested by either tightly constraining or entirely eliminating positive actuator work.

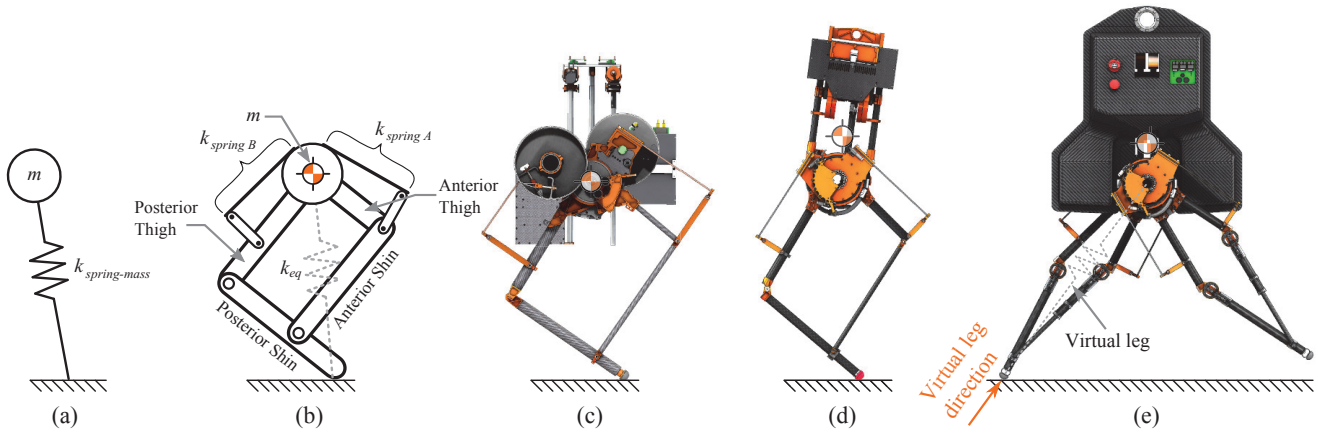

Figure 3: The design evolution of ATRIAS from simple model to single-legged prototype to full biped. (a) spring-mass model for legged locomotion (b) ATRIAS model with naming convention of the four-bar linkage members (c) first-generation prototype monopod (Grimes et al. 2014) (d) final prototype monopod (used for experiments in sections 4.2.4 and 4.3.3) (e) ATRIAS, a bipedal instantiation of the spring-mass model, complete with lateral actuation and inertial measurement for fully 3D locomotion.

by the controlled acceleration of its associated motor, which includes the significant inertia of its rotor and transmission. These factors, among others, are potential contributors to the large power draws in many humanoids. So while quadruped robots have recently made significant economy gains (Seok et al. 2013; Spröwitz et al. 2013), versatile bipeds, such as humanoids, still have energy transport costs an order of magnitude greater than their human counterparts (Collins et al. 2005).

2.2 Passive-Dynamic Robots

Another class of bipedal robots locomotes with only little or no actuation utilizing the passive dynamics of the mechanical system. While exhibiting very efficient locomotion, their action is limited to few gaits and very specific environmental conditions. This class comprises the *passive dynamic walkers* (Collins et al. 2005) and their motorized offspring, the design of which was driven by the inverted pendulum model for walking (McGeer 1990). Delft's robots Flame and TUlip are the largest scale implementations of this approach, standing 1.2 m tall and weighing 15 kg, both were able to walk at 0.45 m/s (Hobbelen et al. 2008). The most energy economical example is the Cornell Ranger, which bears the pseudo-biped inverted-pendulum configuration common among passive dynamic walkers, but is sufficiently actuated and economical that it has walked over 64 km (40 miles) on a single battery charge (Bhounsule et al. 2012).

2.3 Compliant Actuated Robots

Few robots incorporated compliance to enhance dynamic capabilities alongside energy efficiency. These bipeds show more or less versatile behavior and a large range of gaits[2]. Among them are the Raibert hoppers (Raibert 1986), the ARL monopod (Ahmadi and Buehler 1999), the CMU bowleg (Zeglin 1999), the Spring Turkey and Spring Flamingo (Pratt et al. 2001), the tendon-like hopping mechanism of KenKen (Hyon and Mita 2002), and the Jena Fox (Renjewski 2012). Other monopedal testbed hoppers have been constructed for the purpose of testing model-based control techniques (Andrews et al. 2011; Byl et al. 2012). Planar bipeds have been built with distal prismatic springs for the purpose of impact reduction (Hyon and Emura 2005). Further, MABEL (Grizzle et al. 2009), a robotic precursor of ATRIAS, has been able to both walk and run while attached to a boom (Sreenath et al. 2013).

ATRIAS differs from these previous compliant machines in two key ways: **1)** ATRIAS' design has additional features that particularly suit it for replicating the dynamics of the spring-mass model **2)** and is fully capable of 3D locomotion (enables practical locomotion). **1)** Most of these prior examples

[2] A notable multi-bipedal example is the hexapod, RHex (Altendorfer et al. 2001), which crawls about on six springy legs.

have mechanical compliance in one degree of freedom per leg (the ARL monopod is a notable exception). This lack of compliance hinders spring-mass model behaviors, which assume no rigid degrees of freedom (leg rotation is zero-torque and leg extension is compliant). This rigid degree of freedom also impedes the bandwidth necessary for creating these forces virtually via stiffness or impedance control (Kemper et al. 2010). ATRIAS is built with series compliance in both planar actuators for each leg, which allows for more effective force control to render the spring-mass model's zero-torque hip joint (i.e. a pin joint). We demonstrate, with data and model comparisons, that ATRIAS' design, with simple control, replicates spring-mass dynamics in aerial gaits, and more notably from a scientific locomotion standpoint, grounded gaits. **2)** Each of these compliant prototypes have showcased their agility while leashed via power tethers, motivating us to empower ATRIAS with the ability to cut the cord.

2.4 Spring-Mass Model: Dynamics and Control

The spring-mass model was originally proposed as a simplified model for running and hopping (Blickhan 1989). It has been used to model and explain animal locomotion by reducing the system complexity while preserving the general dynamics (Farley et al. 1993; Blickhan and Full 1993; Dalleau et al. 1998). The use of highly reduced-order models to describe dynamical systems for legged locomotion on land and to investigate control strategies was formalized by (Full and Koditschek 1999), termed "templates and anchors."

One of the advantageous features of the spring-mass-models is its passive-dynamic stability (Seyfarth and Geyer 2002). Stability analysis has been combined with spring-mass model dynamics to test hypotheses of neuromechanical functions (Full et al. 2002). The use of stability as an objective function for control gave rise to a number of control strategies to respond to various perturbations during locomotion (Seyfarth et al. 2003; Geyer et al. 2005; Seipel and Holmes 2005; Ghigliazza et al. 2003; Daley et al. 2006; Blum et al. 2010; Peuker et al. 2012). The same model has been able to produce bipedal walking gaits (Geyer et al. 2006), reproducing a number of features of animal walking (Lipfert et al. 2012), and could be extended toward control strategies for trunk stabilization (Maus et al. 2010).

Spring-mass locomotion dynamics bear other attractive features, appealing to varied scientific audiences. To roboticists, spring-mass locomotion has a theoretical energy cost of zero, teasing a solution to the cost-of-transport problem in legged robotics. It is also a low-order dynamical system, typically requiring only four state variables, rendering locomotion planning a more computationally-feasible problem. Such advantages have spurred controls researchers to develop an abundance of specialized spring-mass control techniques which could be plausibly employed on a spring-mass robot (Ernst et al. 2012; Andrada et al. 2012; Piovan and Byl 2013). For biologists, spring-mass dynamics serve as dynamical predictors of animal locomotion, modeling organisms from cockroaches (Blickhan and Full 1993), to lizards (Full and Koditschek 1999), to humans (Blickhan 1989), to quail (Ferris et al. 1998). This general scientific interest in spring-mass locomotion suggests that a spring-mass robot could be a blank canvas for implementing long-studied controls concepts and testing biological hypotheses alike.

3 System Design

Rendering ATRIAS into both a dynamically spring-mass and practical robot requires meeting two sets of specifications: 1) approximating key *model features* and 2) reconciling practical *robot design realities*. Approximating ideal model features facilitates the dynamic behavior we require, while "design realities" ensure that the robot is sufficiently actuated, states are measured, components are protected and housed accessibly, and the robot can maneuver outside the sagittal plane (the typical domain of the spring-mass model). We then discuss mechanical phenomena present in the design that notably impact model adherence or overall robot control: geometric power, drive-train efficiency, reflected inertia, and point feet.

3.1 Model-Feature Implementation

Equipping ATRIAS with the dynamical advantages of the spring-mass model entails approximating four of its key mechanical features: 1) a massless leg, 2) compliance between the ground contact and hip joint, 3) restricting leg forces to the virtual leg axis (i.e. zero hip torque), and 4) positioning the robot mass center near the hip joint. These model features

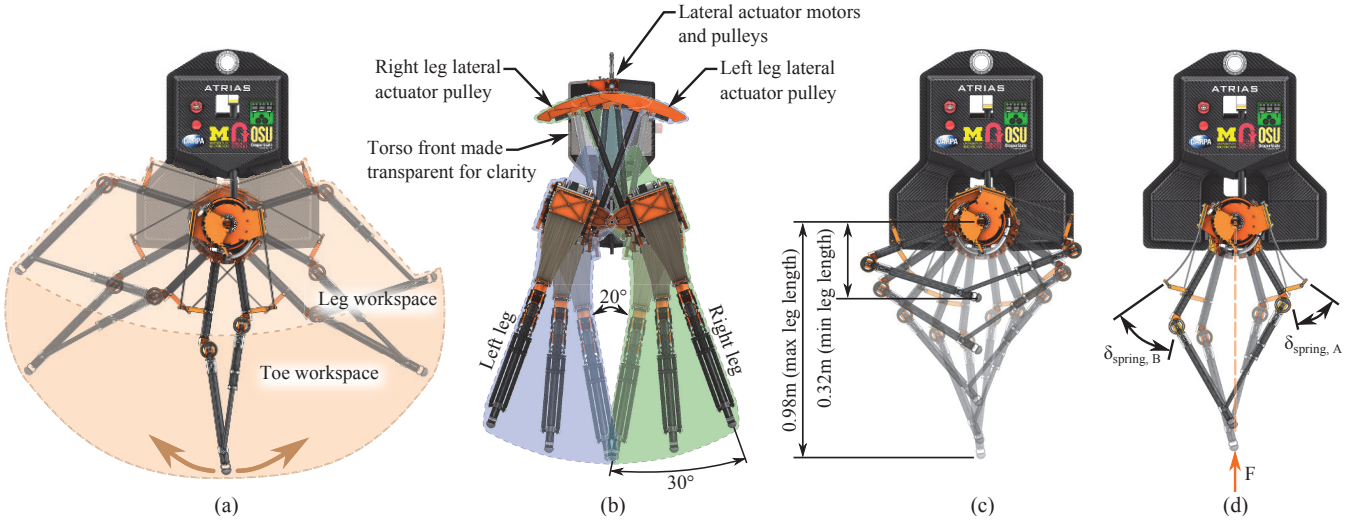

Figure 4: Range of motion and "keep-out" volume of the leg in the (a) sagittal plane and (b) frontal plane. (c) The range of motion for leg length and (d) the maximum kinematic spring deflection until the hard stops are reached.

are primarily achieved as a consequence of ATRIAS' leg mechanism, a two-degree-of-freedom compliant leg (Figure 3b).

3.1.1 Massless Leg

To approximate the massless leg of the spring-mass model, we designed ATRIAS' leg mechanism to be a lightweight four-bar linkage (schematic illustrated in Figure 3b). The linkage has two degrees of freedom, allowing for a large range of motion for the toe in the sagittal plane, as drawn in Figure 4a. The four-bar linkage is constructed of lightweight and stiff carbon fiber with aluminum joints, totaling less than 4% of the robot mass that inelastically impacts the ground with every step[3].

3.1.2 Compliance

Compliance on ATRIAS is achieved mechanically by installing fiberglass plate springs (often called leaf springs), akin to those used in archery bows. By employing mechanical compliance, ATRIAS enjoys the high restitution rates of mechanical springs. In contrast to using virtual compliance approaches (Hogan 1985; Boaventura et al. 2012), mechanical springs alleviate concerns of actuator bandwidth by creating passive dynamics similar to our target dynamics, and spare the inefficiencies of electrical regeneration that would accompany each cycle.

ATRIAS' plate springs bridge the connection between the four-bar leg and the rest of the robot, as visualized in Figures 3b, and 5b. These springs were constructed from fiberglass bar stock because of its high energy density, high coefficient of restitution and stable spring stiffness with temperature, aging, and humidity changes. The springs themselves exhibit an approximately linear spring behavior[4]. When loaded via the four-bar leg, the effective leg spring exhibits a "softening" behavior with respect to the virtual leg length (the mechanical advantage of the linkage wanes as the leg crouches, as illustrated in Figure 4d and later measured in section 4.2.1 and plotted in Figure 9a). This effective nonlinearity in compliance is not intentional, but also no obstruction to ATRIAS' dynamical goals. The springs are mounted such that they can be quickly replaced as needed, or swapped for springs with different stiffness profiles.

3.1.3 Axial Leg Forces

All leg forces in the spring-mass model act exclusively in the axial direction. This feature is a contributing factor for the model's zero-cost gaits and

[3]While a full impact analysis would be intricately state- and posture-dependent, the mass of the components distal to the series plate springs offers a simple estimation, which weigh 2.4 kg, 3.9% of the 62 kg robot mass. This assumes that for most gaits, only one leg impacts per step.

[4]This roughly linear force-length relationship was measured experimentally using a custom-built load-deflection measuring device.

its characteristic underactuated agility. ATRIAS must be able to swing its legs and thus occasionally exert non-axial forces on the leg, but while on the ground (or "during stance" as it is sometimes referred), it must also have the capability to restrict its leg forces to the leg axis. The legs' series-elastic parallelogram mechanism configuration provides a means for ensuring only axial forces that is rather intuitive. If the net torques on each of the proximal leg links are equivalent, there is no tangential force on the leg. So, via a simple controller which regulates the two spring torques into equivalence during stance, ATRIAS' forces are rendered effectively axial. The two degrees of elastic actuation make the linkage better suited for minimize tangential forces via control, because small errors in motor position result in lower forces errors when the system is compliant (Kemper et al. 2010). This manner of restricting forces is implemented in two latter-described hardware tests: passive walking (Section 4.2.3) and the passive throw (Section 4.2.4)

3.1.4 Hip-Centered Body Mass

In the spring-mass model, all mass is lumped into a hip-centered body. As the center-of-mass drifts away from the position of the hip joint, axial leg forces will induce increasing net moments on the torso, causing the body to pitch. For ATRIAS, we required the center of mass to be near the hip point to mitigate torso pitching.

Two design choices most affect this mass location: the proximal location of the leg drive assembly and the arrangement of torso components. First, the leg drive assemblies for each leg weigh 14 kg (28 kg in total), significantly more than weight of the entire torso (22 kg), and the drives' mass centers are just 2.9 cm above the hip point. This distribution makes the mass-center difficult to offset significantly. Second, as shown in Figure 6b, the torso is shaped such that several components can be mounted at or below the hip point, partly balancing the necessarily high placement of the heavy lateral actuators. Consequently, the center of mass of ATRIAS is only 17 cm above the hip even with the torso included, which has proven to be a manageable location in other walking experiments with ATRIAS (Ramezani et al. 2013).

3.2 Robot Realities

While essential math model properties are approximated with the above features, there is a necessary set of requirements for the robot to function, untethered and unsupported, in the real world. These include sensing and measuring forces, the software and electrical system, actuation, and component housing and protection. Further, we describe compromises with the spring-mass model dynamics that emerge from practical robot design, particularly the presence of large rotor inertias.

3.2.1 Actuation

ATRIAS is driven by six actuators in total, *i.e.*, three actuators dedicated to each of its legs. Within these actuator trios, two "leg motors" drive the sagittal motion of the leg through an elastic connection to the leg linkages, while the third "hip motor" directly controls the leg's abduction and adduction (Figure 5a).

The paired leg motors each drive one of the anterior and posterior thigh members through an in-series plate spring. Movement can be coordinated to achieve changes in leg length or leg angle, Figure 4 (a) and (c). This configuration combines torques synergistically between the motors when extending/retracting the leg during high-axial-force maneuvers, such as jumping.

The leg motor pairs are rendered series-elastic by plate-spring connections to their respective linkages (Figure 5b). ATRIAS' series-elastic actuator design deviates from preceding examples (Robinson et al. 1999) in that ATRIAS' springs are designed to store a significant amount of energy relative to the total mechanical energy in the gait. For perspective, during a single-legged hopping test (Section 4.3.1), the plate springs have stored as much as 90 J in one leg, the equivalent mechanical energy of the robot hopping with 15 cm of total vertical travel.

The leg motors were selected specifically for their high torque density (Emoteq Corp.). High motor torque was important in order to limit the size of the necessary gear reduction. The higher the gear reduction, the higher the effective rotor inertia (Section 3.3.3) as well as the potential footprint of the transmission. The leg motors were paired with 50:1 compact harmonic drive transmissions (Harmonic Drive, LLC), further amplifying torque (assembly depicted in Figure 5c). This transmission has minimal back-

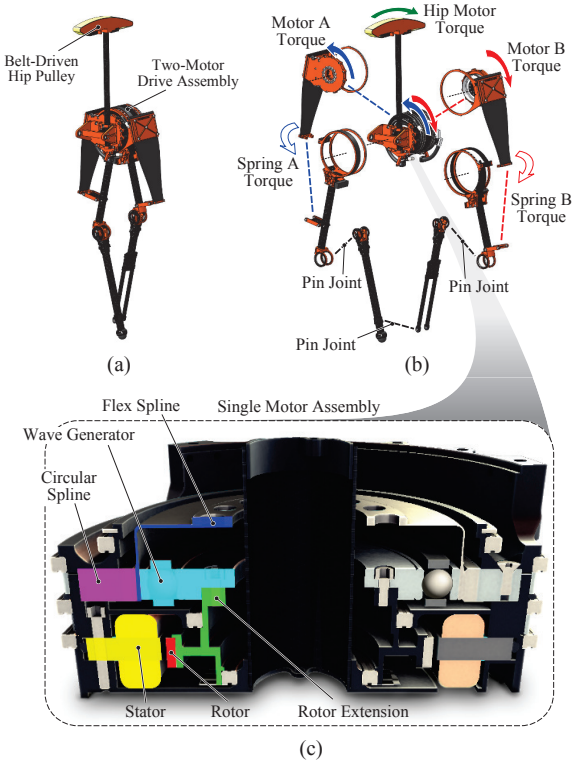

Figure 5: (a) The assembled ATRIAS leg mechanism, actuated in-plane by a two-motor stack assembly and rotated in the frontal plane through a pulley connection to a third motor. (b) The exploded leg assembly, diagramming the kinematic connections from the central motor stack, through the series springs, to the four-bar leg mechanism. (c) A cross-sectional view of one of the paired leg motors, including the transmission via harmonic drive.

lash and also makes the actuator assembly very compact, allowing more room around the hip joint to mount leg assemblies to the torso.

For lateral motion, the "hip motors" extend the planar leg into a 3-dimensional workspace, as illustrated in Figure 4b. Each hip motor is placed high up in the torso and drives a pulley segment on a large lever arm, creating a 56:1 gear ratio. A timing belt is used between the pulleys for the benefits of high force capacity, ease of assembly, and zero backlash.

3.2.2 State Measurement

Control of ATRIAS is most feasible when all states are measured, both actuated and unactuated. In addition to the standard practice of mounting encoders to each motor rotor, ATRIAS employs high resolution sensors to measure the spring deflections and the state of the robot in the world frame, all degrees of freedom which on ATRIAS are underactuated (Spong 1998). For a comprehensive accounting of ATRIAS' sensing components, see Table A.1.

Due to ATRIAS' series elasticity, the force generated by spring deflections is paramount to the gait dynamics, effectively dictating the robot's trajectory. This makes spring deflections high-value state information to capture. Deflections of each fiberglass plate spring are measured by a set of two high-resolution absolute encoders (32-bit), which consequently enables accurate force measurements.

Position and velocity in the world frame are dominant in defining gaits, but for ATRIAS, these degrees of freedom are non-trivial to measure. Many humanoid robots move using flatly planted feet, which gives them an absolute point of reference to measure their velocities in world coordinates. In contrast, ATRIAS has point feet which can be at a range of angles during stance, and thus foot orientation cannot be used to easily infer the robot's state in the world frame (with only proprioceptive measurements). We include a high-precision inertial measurement unit to estimate the robot pitch, angular velocities, and integrate the cumulative Cartesian motion during unrestrained locomotion.

3.2.3 Software and Electronics Specifications

The design of the integrated electronics and software subsystem was driven by a design decision to use available commercial hardware and open-source software. Sensor processing and motor control is facilitated by a number of microcontroller-enabled (ATmega128, Atmel, San Jose, CA, USA) electronic stacks that are connected via EtherCAT-bus to a commercial computer (Mini ITX, i1000A, OEM Production, San Francisco, CA, USA). The control system runs at 1000 Hz on a real-time linux kernel[5] and was developed using Robot Operating System (ROS) and the Orocos framework. A detailed description of the electronics/software system design is available in (Peekema et al. 2013). Each motor and the associated sensors, among them 32-bit linear encoders (RL32BAT, Renishaw, Wotton-under-Edge, UK), limit switches and thermal sensors (See Table A.1), is controlled by one electronic stack, placed in

[5] 99.9% of control cycles are clocked within 41 µs of the mean 1 ms sampling period, demonstrating low jitter.

the body (see Sec. 3.2.4).

3.2.4 Component Housing and Protecting

In the case of a potentially damaging fall, internal components are protected by a shell-like body structure. This body is constructed using composites and composed of two halves. To bear the impact, a stiff and strong structure is made from carbon fiber with balsa core and fiberglass inserts for mounting points, Figure 6a. The other half of the body shell is a non-structural and lightweight cover made from carbon fiber with no core. The resulting shell is designed to be strong enough to shield internal components from incidental damage and prevent wires from snagging when disturbed by kicks, pushes, etc.

The components are bolted to the structural half of the body and are accessible when the cover half is removed. Stiffness of this body structure was important to ensure any body-mounted inertial measurement unit would suffer minimal kinematic flexibility, which would add noise to sensitive measurements. The top of the body features a lifting eye for use with the robot support boom (described in Section 4.1) or an overhead gantry system for catching the robot in the case of falls during troubleshooting and experimentation.

In the event of large lateral forces on the leg beyond the design limit, the knee allows for a controlled break of the leg by way of a mechanical fuse, as shown in Figure 7. The four-bar leg is inherently strong in plane and more flexible when loaded out-of-plane. Use of nylon pins and screws allow the lower limbs (the anterior and posterior shins) to break away cleanly to the left or right. These pins and screws are easily and quickly replaced. Strain gauges are installed at the knee which measure these lateral forces on the leg. By measuring this lateral force, the lateral actuator could be used to actively reduce this force, keeping the toe forces in plane with the leg where it is strong.

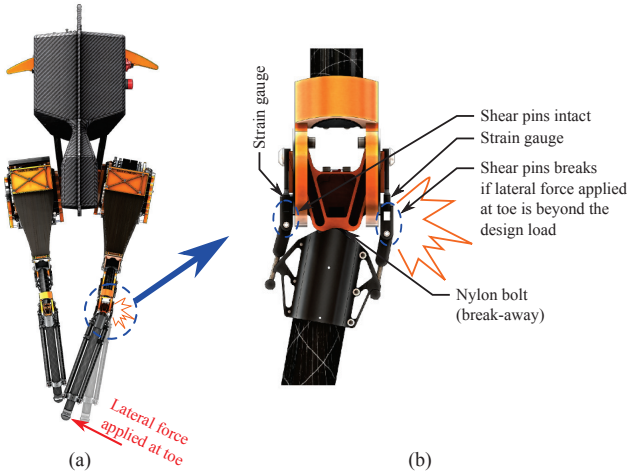

Figure 7: When a lateral force, F, is applied at the toe that exceeds the designed failure point a set of plastic shear pins break allowing the leg fall away and prevent higher loads from damaging other, more expensive components. Strain gauges are included to measure and control the magnitude of these lateral forces.

3.3 Design Discussion

3.3.1 Geometric Power

A fundamental consequence of ATRIAS' leg configuration is a wasteful expense of internal power, so-called *geometric power* (Waldron and Kinzel 1981). With two motors driving the four-bar linkage leg, swinging the leg while loaded requires each motor to perform nontrivial positive and negative work respectively, even if no net work is performed on the robot's mass center. In essence, geometric power is purely overhead, i.e. does not contribute to the mechanical energy of the gait. This phenomenon, plotted in Figure 8, results from the leg-load sharing of the two motors and is inherent to the ATRIAS configuration. Electromechanical regeneration mitigates this overhead to a degree, as ATRIAS' regeneration efficiency is calculated to be between 30 and 40%. For measurement methods and more in-depth power analysis, see Appendix A.

3.3.2 Drive Train Efficiency

The choice of a harmonic drive transmission also comes with a mechanical efficiency cost. A prior iteration of the ATRIAS leg included an epicyclic cable drive (Grimes et al. 2014), but was removed due to its large keep-out volume (total volume swept by the mechanism, corresponding to all points in the end-effector workspace) which overly limited the space available for torso volume. Torso volume was particularly important for housing all the components necessary to make ATRIAS 3D-capable. While harmonic drives are sufficiently compact, they also have lower mechanical efficiencies, typically around 50-80% (compared to the cable drives of predeces-

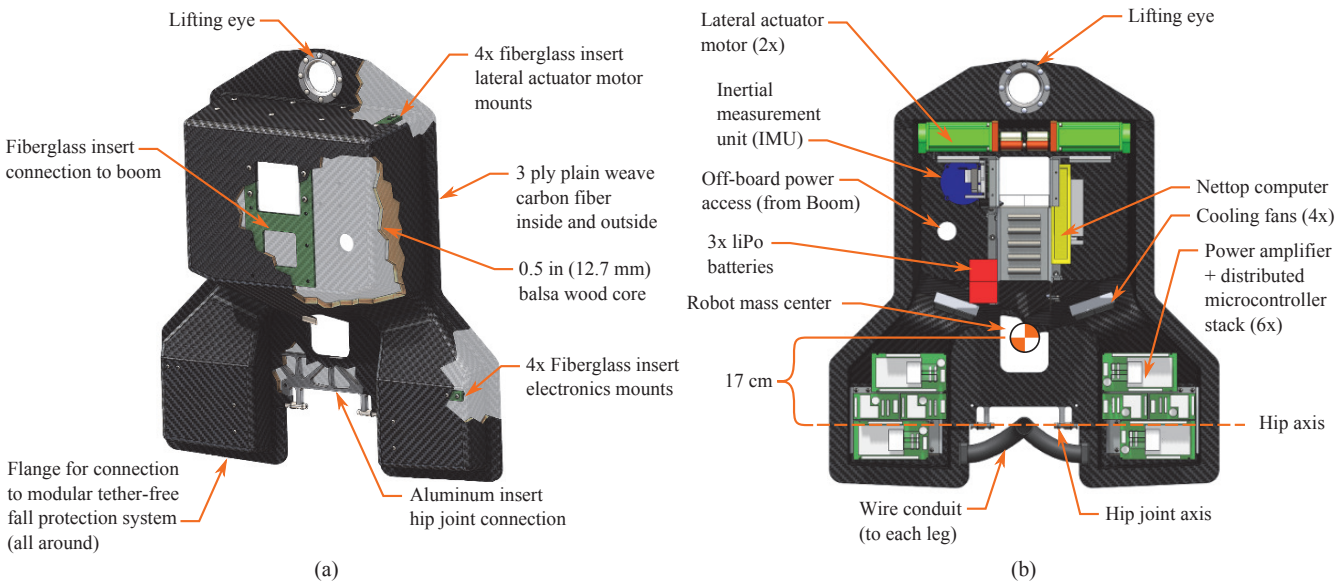

Figure 6: (a) Construction details of the body to make it a strong protective shell to house the various components of the robot (cover half not shown for clarity). (b) Layout of components secured to the structure half of the protective body shell.

sors MABEL and ATRIAS 1.0 of 94%). These losses likely exacerbate ATRIAS' mechanical transport costs.

3.3.3 Reflected Inertia & Torso Eccentricity

When regulating its angular orientation, ATRIAS must contend with both the lever arm of its torso mass and the inertia of its spinning rotors. Acceleration of the sagittal motors exerts significant reaction torques on the torso as a consequence of so-called *reflected inertia*. While the rotor inertia for each of the sagittal rotor assemblies is rather small, $0.0019\,\mathrm{kgm}^2$, when transmitted through a 50:1 harmonic drive, the reflected inertia scales with the square of the gear ratio, *i.e.* a 2,500-fold increase. Consequently, when the two leg motors accelerate in concert (such as in swinging motions), their combined reflected rotor inertia sums to $9.50\,\mathrm{kgm}^2$. This effective inertia is massive, totaling twice the hip-centered inertia of all non-rotor components ($4.65\,\mathrm{kgm}^2$). Such inertial effects are a considerable drawback of large gear reductions in general, and harmonic drives is particular (which are commonly manufactured with gear ratios of 150:1 or higher).

However, effects of rotational inertias on torso pitching are mitigated by leg recirculation. It is generally uncommon for a gait to require both legs to swing in the same direction, thereby canceling at least a portion of the inertial effects. Further, the resulting reaction torques have not prevented successful walking in practice, as multiple controllers have regulated the torso position of ATRIAS while walking (e.g., both with torso angle controlled steady (Ramezani et al. 2013) and with the torso pitching significantly (Hereid et al. 2014)).

Reflected inertia also brings deleterious effects on actuator performance for certain tasks, such as force control. There are occasions in which it is likely useful for a robot to regulate its leg forces (as demonstrated by "hopping in gravel" in Section 4.3.3), which high rotor inertia is known to impede. Specifically, this inertia enforces an effective motor acceleration limit, which curtails the actuator bandwidth for accurately rendering desired forces (Kemper et al. 2010). While the ATRIAS leg is still capable of some demonstrative and useful feats of force control (Figure 16), such large inertia is likely the main limiting factor of ATRIAS' actuation scheme.

3.3.4 Feet, in absentia

Unlike many of its robotic counterparts, ATRIAS has no actuated feet, nor feet of any meaningful sort. Its legs terminate with simple rubber nubs, approximating point feet. This, of course, is by design as the spring-mass model is point-footed. However, this makes standing still non-trivial as point feet have no

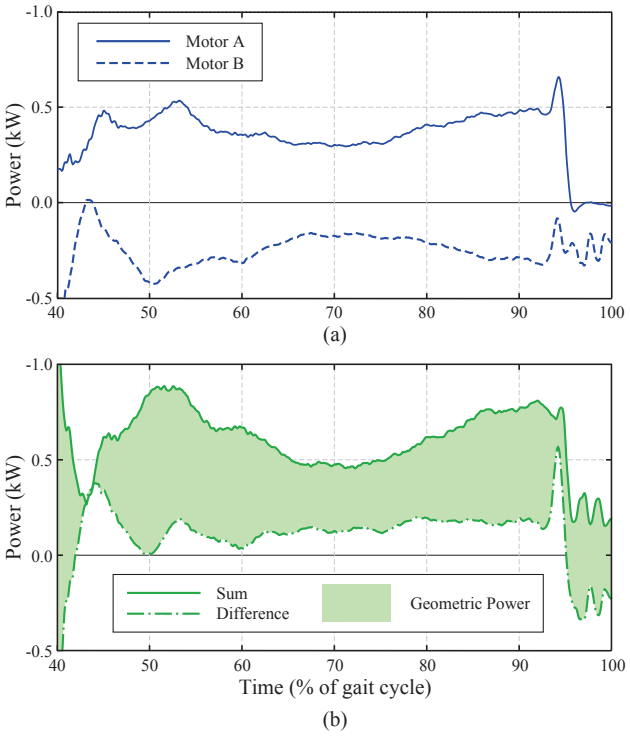

Figure 8: (a) Instantaneous power generated by motors A and B during stance phase of a walking gait, as described in Section 4.3.2. Motor B is producing negative power for the duration. (b) The sum ($|A| + |B|$) and difference ($|A| - |B|$) of the absolute value of mechanical power produced by motor A and B. The shaded region represents geometric power, a byproduct of the four-bar leg and motor configuration. When swinging the leg while axially loaded (i.e., during stance phase), geometric power acts as power overhead, exacerbating energy costs. These power estimates were calculated by measuring spring deflections and motor velocities, and are described in further detail in Appendix A.

effective polygon of support. This means ATRIAS must adopt more dynamic approaches to stability, such as taking a stepping to recover from falls (Pratt et al. 2012; Stephens and Atkeson 2010).

For traversing a fully three-dimensional environment, some form of contact pad can be helpful for resisting yaw accelerations. This would prevent ATRIAS from spinning like a top and has been shown to be usefully stabilizing in 3D simulations (Hamed and Grizzle 2014). As such, we prototyped lightweight passively-pivoting contact pads for use in our 3D-stepping experiment (Section 4.3.4). The pad is 10-*cm*-long, 2.5-*cm*-wide fiberglass sheet with rubber nubs attached under each end. The pad freely pivots in the sagittal plane to conform to the orientation of the ground upon touch down, and elastic bands act as a return spring to reset the pad angle upon lift-off. Each pad is sufficiently lightweight and loosely sprung that it can easily flicked with a finger. As such, it has no apparent effect on sagittal plane spring-mass dynamics, but effectively curtails yaw accelerations. In short, this addition in 3D experimens (Section 4.3.4) does not compromise our spring-mass design intent.

4 Experiments

Assessing the design of ATRIAS requires validation on two fronts: 1) the degree to which its passive dynamics match the spring-mass model, and 2) its dynamical capabilities, or agility, when actuated. After explaining our experimental setup in Section 4.1, Section 4.2 validates ATRIAS' spring-mass behavior with a number of passive tests. In these passive tests, actuation is either thoughtfully limited or eliminated entirely in order to isolate ATRIAS' passive dynamics, and compare them to the spring-mass model. Section 4.3 demonstrates the capacity of ATRIAS to perform a variety of sustained dynamic maneuvers while retaining key features of its passive motions. For additional details about the controllers for these experiments, see Appendix C.

4.1 Experimental Setup

In pointedly testing ATRIAS' dynamical features, experiments were conducted while constraining its motion to a roughly planar workspace. Such restriction facilitates a more controlled test of ATRIAS' actuation capacity and spring-mass properties (which primarily manifest in the sagittal locomotion plane). This approximately sagittal constraint was achieved by connecting the torso to a pivoting boom.

The boom offers a 2.0-meter turning radius and three degrees of freedom: boom azimuth, boom altitude, and robot pitch (each can be individually locked or freed). This spherically constrained motion approximates sagittal-plane locomotion for large radii (Colett and Hurst 2011). Further, these three rotational axes are measured with encoders, allowing measurement of the world-frame for both experimental analysis and feedback for real-time control. All state information from the boom is collected using the same software/electronics infrastructure as

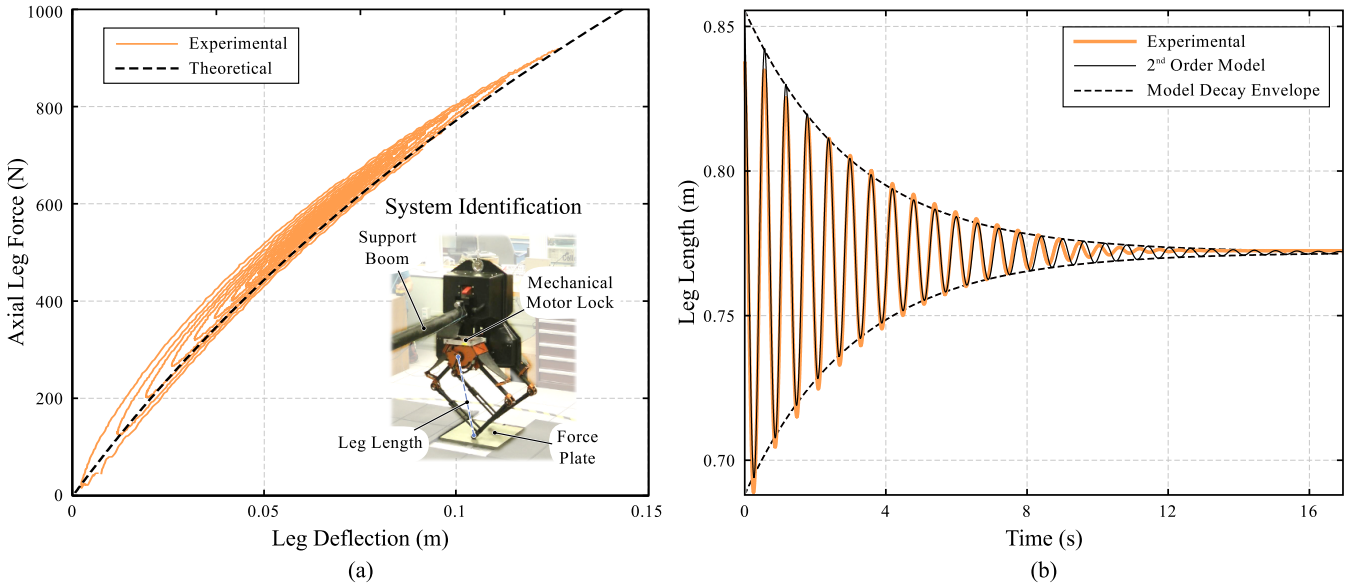

Figure 9: (a) ATRIAS' force-length curve, measured via a system identification test, where the robot is bounced on one leg and forces are measured by a ground-mounted force plate. The experiment shows a close match between the loading edge of axial leg force measurements (thin, solid line) and the theoretical force-length curve derived from leg kinematics (thick dashed line). The rest length of the leg is $0.9m$ during the test. The figure also includes a labeled photograph of the experimental setup. (b) The decaying oscillation of the dropped robot and its fitted curve (computed using a second-order oscillation model) which show close agreement. Figures 9a and 9b present data from the same drop test.

the robot, recorded at the same 1 kHz control rate.

To minimize unintended interference in experiments, the boom is designed with minimal rotational inertia and rotational friction. The boom's two protruding rods, for constraint and catching respectively, are constructed with carbon fiber tubes, helping limit the boom's rotational inertia to just 4.3% of the boom-robot system. To limit friction, the rotational joint is a four-point contact ball bearing, with any routed cables connected through a low-friction slip ring[6]. The resulting drag force against the robot is estimated to be less than 1 N, only 0.2% of ATRIAS' body weight.

Further, the boom is designed with other practical functions for robot experiments. To raise the robot for drop tests, the boom provides a motor-driven hoisting line, allowing for both easy lifting and more precise test replication. To provide safe and clean drops, a quick-release mechanism connects to the robot and is disconnected via a swiftly pulled pin. The boom also serves as a safety mechanism, catching the robot on an independent slack line if the torso dips too low.

When possible, ground reaction forces are measured with a force plate that is mounted flush with the laboratory floor. Typically used in biomechanics labs for gait analysis, this force plate (OR6-7-4000, AMTI, Watertown, MA, USA) measures forces (x, y and z) and moments (M_x, M_y and M_z) at a sampling rate of 1 kHz. Force plate measurements are synchronized to the robot's data collection system by means of an electronic triggering signal. Measuring spring deflections provides another mode for force reporting, which is particularly apt for logging multi-step maneuvers for which the single force plate spans an insufficient surface area. Each experiment indicates which manner of force measurement was employed.

Some experiments and demonstrations were performed using the monopod prototype of ATRIAS shown in Figure 3d. The monopod leg design is nearly identical to the ATRIAS biped, differing primarily in torso configuration (and of course, includes only one leg). Most relevantly, the monopod weighs only 30 kg, just under half the biped's 62 kg weight, better suiting throwing experiments (Section 4.2.4)

[6]While the presented experiments used an off-board power tether, the robot can function fully untethered, using on-board lithium-polymer batteries and computing, with wireless communication to a user-interface computer.

and testing the most dynamic maneuvers (Section 4.3.3).

4.2 Model-matching Validation

4.2.1 Identifying Spring-Mass Behavior

One straightforward way to assess ATRIAS' spring-mass dynamics is by identifying a force-length relation and a decayed oscillation model for the robot. Using mechanical stops, we locked the ATRIAS' motors in place and disabled control, permitting a fully passive robot test. We configured the support boom to restrict torso rotation and horizontal motion, allowing only for the vertical oscillation of a spring-mass system. Using the boom's winching cable, we raised the robot slightly off the ground and dropped it.

In Figure 9a, we see the resulting force-length curve, resembling a nonlinear spring with a softening behavior. This softening curve is an expected feature of ATRIAS' leg configuration, where the apparent falling-rate leg length stiffness results from the nonlinear geometric relations inherent to the fourbar linkage. We can see the previously derived theoretical force-length relation (Grimes et al. 2014) matches very closely to the loading side of the experimental curve. On the unloading side, we see hysteresis associated with dissipative losses that must be offset through actuation.

We can determine the magnitude of this dissipation by examining the decay of the spring-mass oscillations. We fitted the experimental data to a linear damped spring-mass model with one degree of freedom. Figure 9b illustrates a comparison to the fitted model parameters[7], $m = 59.9\,\text{kg}$, $k = 6.543\,\text{kN/m}$, $c = 38.0\,\text{Ns/m}$, and $\zeta = 0.061$. This damping ratio is relatively small, suggesting ATRIAS' springs are reasonably efficient energy storage mechanisms. However, this analysis does not include the losses from an impact.

4.2.2 Passive Drop

While the previous analysis estimates the dissipation in ATRIAS' springs, a number of other phenomena in the passive system can contribute to energy losses in legged robots (*e.g.* impacts, friction, backlash). In this test scenario, we evaluate the magnitude of these combined losses from the passive system (including spring dissipation) through passive bouncing. We constrained movement to the vertical direction and dropped ATRIAS from a fixed height (5 cm) with a mechanically fixed leg length (84 cm), allowing the springs to absorb the impact.

After the drop, ATRIAS bounced into an airborne state three times before settling into a grounded state, as shown in Figure 10. When dropped from 5 cm, the robot returns to a height of 2.4 cm on the next apex. By examining the potential energy lost between these subsequent apexes, we determine a

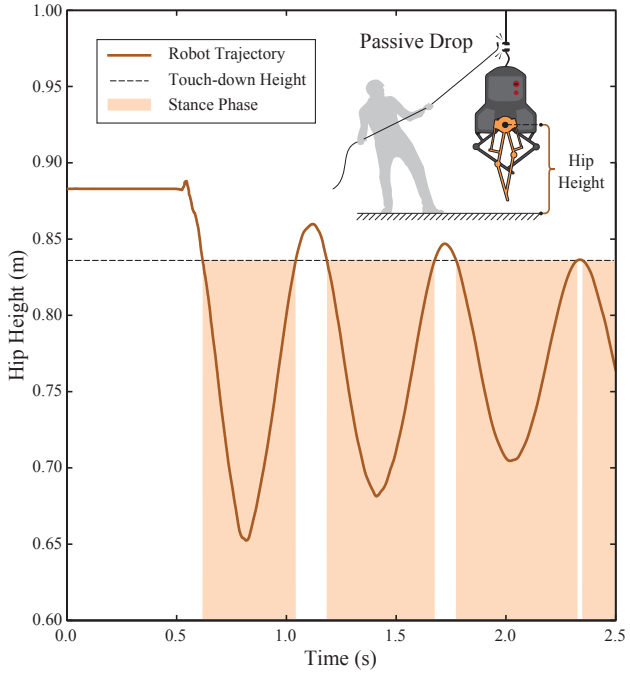

Figure 10: A passive drop experiment, designed to elicit the robot's passive spring-mass dynamics as expected in hopping gaits. ATRIAS is dropped onto its unpowered leg with its motors mechanically locked, isolating the passive plate springs as the single of spring-mass dynamics. The center of mass position (solid line) exhibits a "bouncing" trajectory characteristic of a spring-mass system. Periods of ground contact, i.e. the stance phase, (shaded region), and the threshold height where ATRIAS makes ground contact (dashed line) are also visualized. An illustration depicts the passive drop experimental setup, the support boom constrains the body rotation and all non-vertical motion, and ground-reaction forces are measured by a force plate. Video shown in Extension 1a.

[7]Reported values for robot mass that vary slightly across experiments are due to the inclusion/exclusion of the onboard battery pack.

coefficient of restitution of 0.69. This suggests that ATRIAS' leg mechanism has the capability to return as much as 48% of the energy to a dynamic gait (such as hopping) that would be otherwise lost in a plastic collision.

4.2.3 Passive Walking

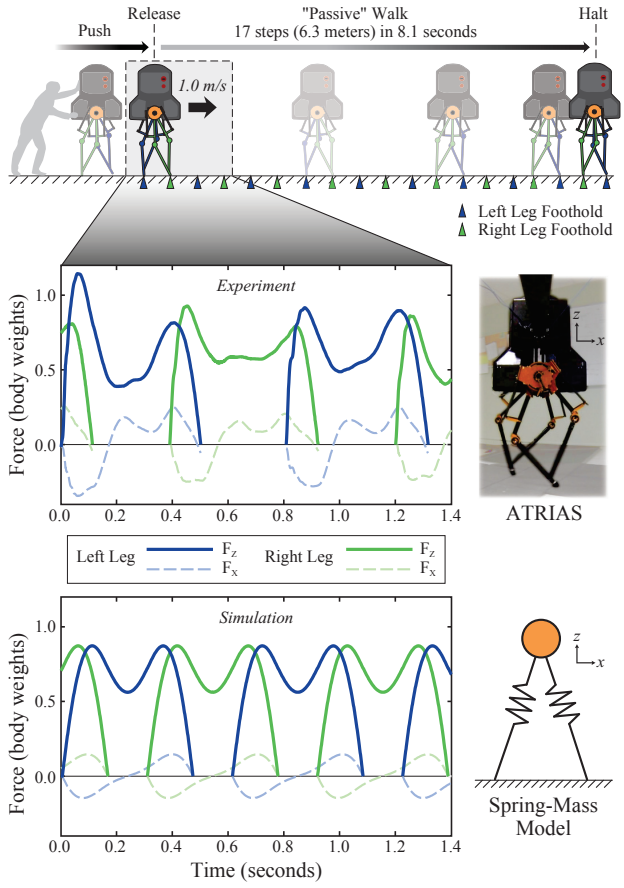

Figure 11: A "passive" walking experiment, where ATRIAS is pushed, released, and walks until it stops from energy dissipation (cartooned at top with measured foothold locations). Ground-reaction forces for ATRIAS (middle) are compared to a simulation of the spring-mass model (bottom), showing a number of qualitative similarities, including the characteristic double-humped vertical force. Using a controller designed to reciprocate its legs while avoiding performing work on the robot CoM, ATRIAS walked a notable distance of 6.3 meters over 17 steps before stopping. Video shown in Extension 1b.

This experiment evaluates whether ATRIAS' passive dynamics exhibit spring-mass walking dynamics in low-energy gaits. Particularly, we are looking to see if ATRIAS will exhibit the characteristic double-humped ground reaction force associated with spring-mass walking, and by extension, human walking (Geyer et al. 2006).

Unlike the passive drop test, in order to walk, ATRIAS' motors must be unlocked and able to swing. However, in order to approximate a passive robot test, we employed a controller that reciprocates the legs while avoiding performing any instantaneous net work on the robot. During a leg's stance phase, the phase with the most potential for significant energy exchange, the two leg motors regulate two key outputs to facilitate passive spring-mass dynamics: the net leg torque (which is driven to zero) and the set point of the virtual spring (which maintains a nominal position). The net leg torque is zeroed by controlling the spring deflections to be equivalent, as suggested in Section 3.1.3. A second controllers simultaneously controls the position of the virtual spring set point. This was accomplished in the prior experiments (Sections 4.2.1 and 4.2.2) by mechanically locking the motors at a specified separation distance, which we now also achieve using position control on the motor angles (See Appendix C for mathematical formulation of the controller).

During swing phase, the controller positions the leg to a touchdown angle which would yield limit-cycle walking for the spring-mass model. Such touchdown-angle-driven control has been used to control spring-mass models (Ghigliazza et al. 2003), incidentally demonstrating ATRIAS' potential amenability to spring-mass control techniques. At the beginning of leg swing, a position controller drives the swing-leg's toe position along a spline, tracing a path between the current position and the desired leg angle. Again, for this test, the robot was mounted to the boom with the torso rotation locked as this is a test of spring-mass dynamics, not torso regulation or frontal stabilization.

After a human operator pushed ATRIAS to a 1 m/s walking speed, ATRIAS was released and continued to walk for 6.3 m over 17 steps before slowing to a stop as illustrated in Figure 11. Propulsion was also added by tracking errors in our zero-leg-torque control (averaging approximately 31 N (7 lbf) of net horizontal force at the toe).

The passive walk test produced the typical double-humped ground reaction forces of the spring-mass model (Figure 11). More notably, the experimental data fits well with a simulation of the spring-mass model, simulated using ATRIAS' mass, spring-

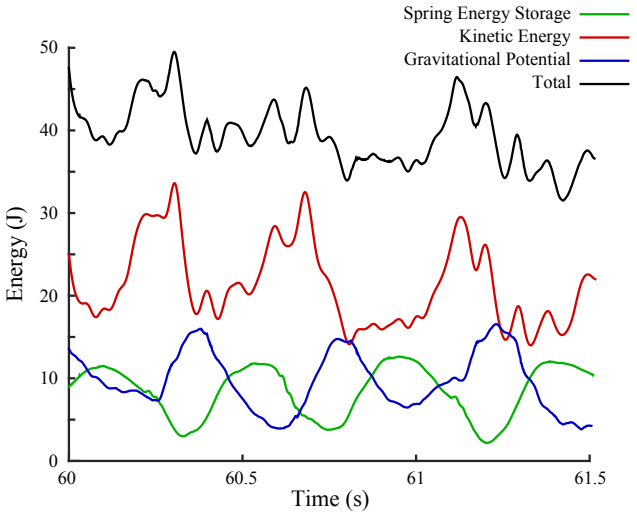

Figure 12: A plot of the energy being cycled through the gait during the pushed-release-stop walking test, showing that significant energy is exchanged between spring storage, gravitational potential, and its motion. Total energy decreases as the gait slows to a halt. Non-conservative effects result from dissipative losses (likely primarily molecular damping in the spring, ground impacts and friction) and the error dynamics of the actuators from attempting to track zero stance torque.

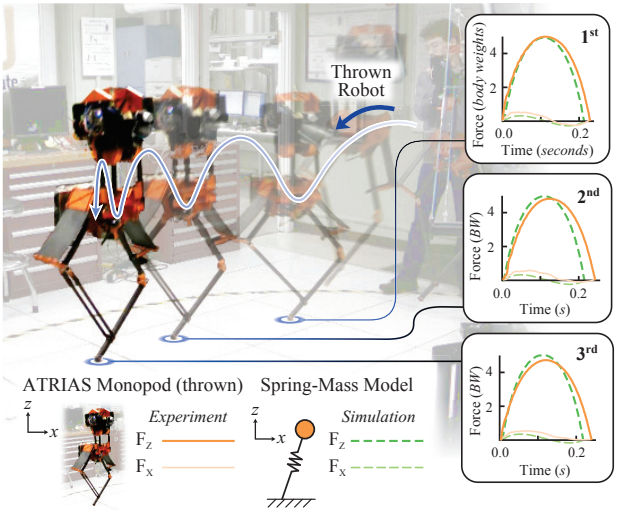

Figure 13: The ATRIAS monopod prototype being tossed to observe its passive dynamics while hopping or running. The monopod completed five hops before falling. For the first three hops, the ground reaction forces of the robot (solid lines) closely matched a simple spring-mass model (dashed lines) with the same parameters and initial conditions. Video shown in Extension 1c.

function, and initial conditions. This demonstrates that spring-mass walking dynamics can be the dominant dynamics of ATRIAS. Further, the correspondence between the robot and model by enforcing leg angles used in the simple model suggests that ATRIAS is a well-suited platform for spring-mass control policies.

This walking test also shows that the springs play a significant role in the energetics of the walking gait. In Figure 12, we plot the kinetic, gravitational, and stored spring energy of the robot when walking. Within a step, ATRIAS' kinetic energy fluctuates with an amplitude of $14.6 \pm 2.44J$ during the spring-mass gait cycle, and gravitational potential swings $11.7 \pm 1.96J$ with each rise and fall of the robot's mass. The springs store and release $10.4 \pm 1.81J$ in each step, a very similar magnitude to both gravitational and kinetic energy. This demonstrates that the springs are a significant energetic participant in the cycling between kinetic and potential energy during locomotion, evidencing ATRIAS' embrace of spring-mass locomotion dynamics.

4.2.4 Passive Throw (Monopod)

To elicit ATRIAS' passive dynamics in aerial gaits such as hopping and running, we connected the ATRIAS monopod to the boom and tossed it, observing its subsequent bounding gait. Like the passive walking test (Section 4.2.3), the leg was actively reciprocated during swing phases, in this case resetting to a constant attack angle. During stance, again, the plate springs were regulated to enforce zero net hip torque while the effective rest length of the virtual spring was held constant, thereby attempting to impart zero net work on the robot (See Appendix C for mathematical implementation). Due to its lighter weight, this test was better suited for the monopod as it is far easier for a human experimentalist to throw. The torso rotation was mechanically locked to the boom.

Upon throwing, the monopod completed five hops before dissipative effects led to a fall. Such successive passive hops provides evidence of ATRIAS' mechanical efficiency even with higher energy gaits, where impacts losses are typically exacerbated. Like in the passive walking experiment, the thrown monopod shows marked similarity to the spring-mass model, as plotted in Figure 13. The ground-reaction forces

display the characteristic single-humped force profile of spring-mass running (as well as animal running). When directly compared to a simulated spring-mass model with the same mass, spring function, and initial throwing conditions, the ground-reaction forces match very closely to the monopod over the first three hops. This degree of model matching indicates that ATRIAS' engineering was significantly successful in rendering spring-mass passive dynamics for both walking and hopping gaits.

4.3 Performance Demonstration

4.3.1 One-Legged Hopping

Hopping represents a high-power mode of locomotion, requiring fast push-off while legs are heavily loaded. For ATRIAS, hopping also serves as a mechanical precursor for the strenuous dynamical demands of running. To validate ATRIAS can handle the rigorous power requirements of hopping and running, we controlled ATRIAS to hop on one leg.

In this test, ATRIAS starts from standing position and begins an uninterrupted sequence of hops with one leg for support. For hopping control, we commanded the springs to generate ground-reaction force trajectories (see Appendix C) associated with a spring-mass hopping model. The boom was configured to lock the torso angle to facilitate this test. Video shown in Extension 1d.

Upon startup, ATRIAS demonstrated notably high hopping heights, which we claim are on-par-with or greater than human capabilities. The biped reached a height of over 9*cm* within the first hop, and continued to hop on the same leg for dozens more cycles with an average toe clearance of 9.6 cm ($\pm$0.9 cm, $N = 55$), as shown in Figure 14. However, a more apt measurement of hopping prowess is the center-of-mass height, which cannot be cheated by rapidly retracting legs during flight. ATRIAS' center of mass, as approximated by the hip point, also consistently clears 9cm over its takeoff height. This is higher than humans hop (less than 4.4 cm) when asked to do so continuously on one foot (Chang et al. 2008) (See Appendix B for detailed analysis). The rate of hopping was also similar as the robot hopping frequency was 2 Hz, very close to the preferred human hopping frequency of 2.2 Hz. Arguably, this hopping frequency was "comfortable" for ATRIAS as well, since the hopping frequency was that of ATRIAS' passive spring-mass model, thereby approximating maximum efficiency. The robot performed this test multiple times, stopping only on command, showing that the hardware is sufficiently high-powered for continuous hopping on just one leg. We claim that this sustained human-height-matching hopping capability is novel for a human-scale robot that can function untethered.

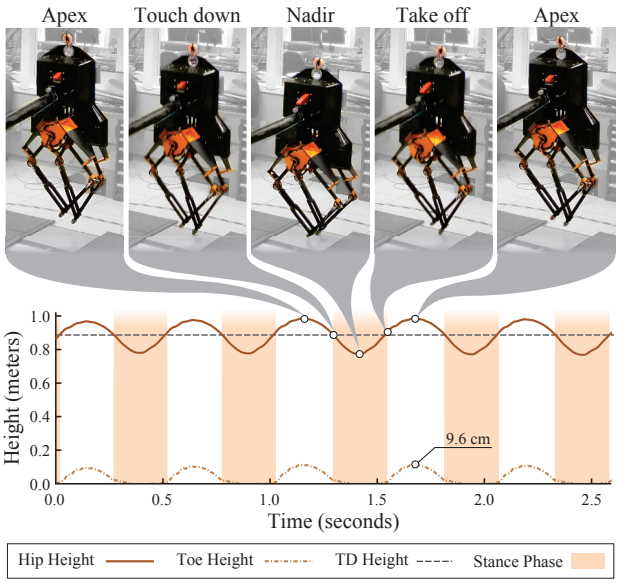

Figure 14: ATRIAS hopping on one leg over more than 50 hops. The toe (dash-dotted line) consistently clears a height of 9.6 cm ($\pm$0.9 cm) and the hopping robot achieved a sustained body trajectory (solid line). Biomechanics measurements suggest that this hopping height is higher than humans typically exhibit on one leg when hopping continuously. The stance-phase (shaded region) duty factor for the hopping cycle is 50% ($\pm$2%), demonstrating non-trivial flight times. Further, five points of interest in the hopping cycle (apex, touch down, nadir, take off, apex) are labeled and shown as performed by ATRIAS. Video shown in Extension 1d.

4.3.2 Sustained Walking

While Section 4.2.3 demonstrated spring-mass walking in the short term with a nearly passive machine, we seek to demonstrate that such walking can be sustained on ATRIAS. To do so, we implemented a controller based on a simple state machine.

The walking controller alternates between stance and swing phases, with each leg occupying the opposite phase of its counterpart. The phase switch is triggered by the leg currently in stance reach-

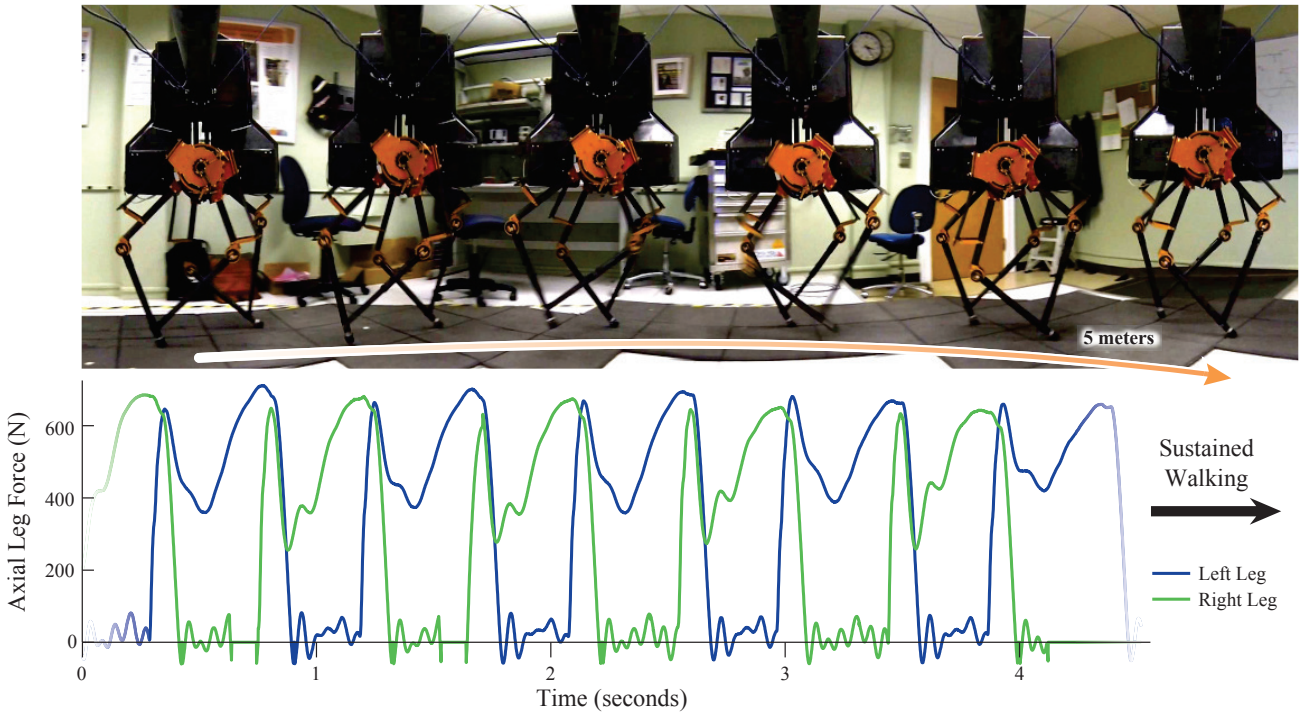

Figure 15: A stroboscopic image of a sustained ATRIAS walking gait and its associated axial leg forces, demonstrating that sustained walking is viable for ATRIAS while sporting the characteristic "double-humped" force profile of both spring-mass walking and human walking. Video shown in Extension 1e.

ing a predefined extreme angle. During stance, the leg has to support and propel the body. The motors generate holding torques allowing the springs to be loaded and to redirect the trunk's vertical motion, thus supporting the robot's weight during the stride. A hip torque is generated by distributing the holding torque unevenly between the motors rotating the leg, propelling the robot forward. During the swing phase, the leg is driven forward, first shortening to ensure sufficient ground clearance and extending again towards the end of swing, culminating in leg retraction when nearing touchdown. Timing of motion and phasing is based on the stance leg motion, introducing a virtual constraint (see Appendix for mathematical control description).

The robot exhibited compliant walking, generating ground reaction force profiles similar to those observed in human walking, as plotted in Figure 15. To our knowledge, this characteristic double-humped force pattern has not yet been reported in sustained robotic walking.

4.3.3 Hops in a Box of Rocks (Monopod)

Nonrigid surfaces and uncharacterized terrain are inevitable in natural environments. As a test of ATRIAS' reflexive capability to handle extreme and unmodeled terrain changes, we challenged the hopping ATRIAS monopod with a pit of pea gravel, *i.e.* a box of rocks. We commanded the monopod to hop vertically on the laboratory floor, and while airborne, pushed it over the pit. This "rocks test" assesses how closely ATRIAS can maintain its nominal mass trajectory despite an extreme disturbance, testing whether ATRIAS' mechanical system is capable of responding to surprises in the real world.

Admittedly, a box of gravel is an unusual robot test, but is an appropriate reflexive challenge in both magnitude of disturbance and unpredictability of terrain dynamics. Extending 16.5 cm beneath the floor, this box of rocks is hazardously deep for a hopping robot, a full 17% of ATRIAS' nominal leg length. Further, while an open-air fall is simple to model and easy to plan for, granular media is notoriously not (Zhang et al. 2013), making a gravel trap an apt analogue for the unknowns of real-world ter-

rain, less befitting of intricate model-informed control design. Further, this gravel is somewhat loosely packed, meaning that ATRIAS will likely sink some portion of the entire 16.5-cm depth of the trap, requiring significant energy injection from the actuators to maintain its hopping height. For this hardware test, the boom was locked to constrain the robot to only vertical motion.

The test controller was designed to regulate the ground-reaction forces, as measured by the springs, tracking the force trajectory associated with its nominal hopping gait. By controlling these forces, in effect, the robot mass trajectory is regulated irrespective of the terrain beneath it. In essence, the controller does not "switch" when on the rocks as opposed to the floor, but merely regulates force as described in Appendix C. Properties of this "force control" technique are elaborated upon other studies (Koepl and Hurst 2013), including it being work-optimal disturbance rejection for dissipative surfaces (Hubicki and Hurst 2012). The rocks were not modeled and neither the controller nor its gains were tuned for these terrain dynamics, so as not to meddle with the reflexive nature of this rocks test.

After over a dozen cycles of steady-state hopping, the ATRIAS monopod was nudged over the rocks. The robot toe plunged into the gravel pit, as shown in the film strip in Figure 16a. ATRIAS regulated its forces by rapidly extending its leg, thereby injecting lost energy. After eight complete hops in the box, ATRIAS jumped out of the pit and resumed its prior steady hopping on the laboratory floor. Figure 16b shows the hopping apex height was largely maintained despite the sizable terrain change. This disturbance is dynamically extreme for legged locomotion, but was handled by the ATRIAS monopod without planning or switching controllers.

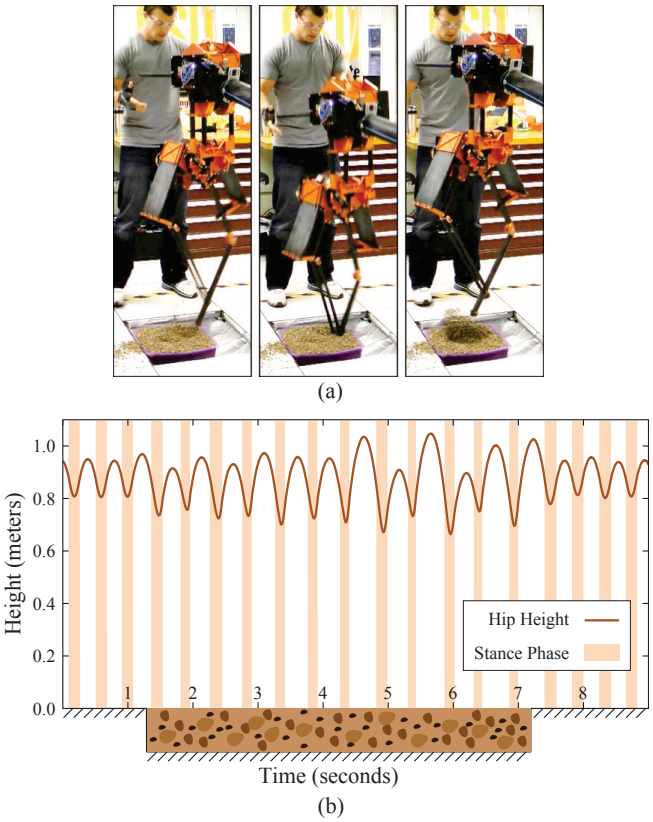

Figure 16: As a test of reflexive actuation in a surprise terrain change, the ATRIAS monopod hopped into, and out of, a 16.5-cm-deep gravel pit. The controller was not switched depending on terrain and the robot was unaware of the impending trap. (a) Images of the monopod plunging into the rock trap. (b) The hip height of the monopod before, during, and after the terrain change, showing it can largely maintain its apex hopping height despite the 16.5 cm depth of the trap. Video shown in Extension 1f.

4.3.4 Dynamic Balancing in 3D

In this balancing experiment, we demonstrate that ATRIAS is mechanically capable of stable 3D locomotion. In particular, this means the robot must be able to move and balance without external support, external power, or communication cables. Four 22V lithium polymer batteries (two in series, two in parallel) were mounted inside the torso, and a wireless bridge provided communication to a user-interface computer. The only connection to any support structure was a slack safety cable, which only becomes taut when if the robot falls due to malfunction.

Using a specially-developed 3D locomotion controller (described in (Rezazadeh et al. 2015)), ATRIAS was commanded to step in place and maintain balance by stepping in place from right foot to left foot repeatedly (Figure 17). During the experiment, ATRIAS was able to balance continuously without signs of instability. This simple experiment demonstrates that ATRIAS' spring-mass design is mechanically capable of practical locomotion, where experimental restraints, tethered power, and wired communication is not possible. Further, the ground reaction forces also manifest in a "double-humped" profile as per spring-mass walking, all while balancing in three dimensions.

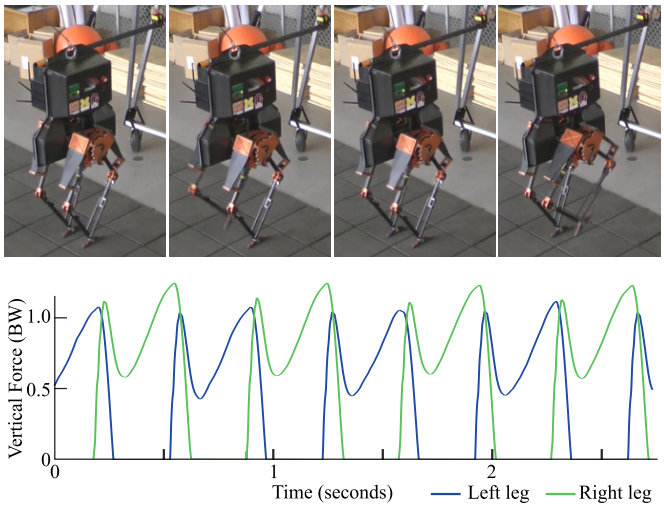

Figure 17: A sequence of tiled images showing ATRIAS marching in place in 3D. Using a controller described in (Rezazadeh et al. 2015), the robot continually steps in place to hold position. Batteries and computers are all mounted onboard, with no communication cables or connection to the experiment boom. A slack safety cable is attached to the top of the torso which would catch the robot in case of a fall. Plotting the vertical leg forces also shows "double-humped" ground reaction forces of spring-mass walking. Video shown in Extension 1g.

5 Future Work

5.1 Leg Configurations and Geometric Power

ATRIAS' four-bar leg mechanism has certain advantages such as being very lightweight, but also clear disadvantages like geometric power. However, there is no inherent reason why other lightweight leg designs must bear these inherent losses. By exploring the space of possible leg configurations, one can identify a kinematic layout that consumes no geometric power for the desired motions that can also accommodate low-weight and compliance (Abate et al. 2015). Given such a leg mechanism, the total mechanical power consumed by the actuators may begin to approach that of the mechanical energy lost during the gait cycle.

5.2 Control

In a broad view, various control frameworks are potentially suited to take advantage of ATRIAS' underactuated dynamics. Hybrid-zero dynamics (HZD) (Westervelt et al. 2003; Ames 2014), receding-horizon differential dynamic programming (Erez et al. 2013), and sum-of-squares verified trajectory libraries (Manchester et al. 2011) are a few examples of control frameworks that can support ATRIAS' high degree of underactuation. More specifically, approaches have also been developed to tackle more biped-specific issues such as torso and frontal-plane stabilization.

While the presented hardware performance tests were performed with locked torso rotation, many solutions exist for handling torso dynamics (some of which have already achieved walking with ATRIAS). Within the framework of spring-mass techniques, the torso angle can be regulated by constraining the direction of resultant leg forces through a predetermined intersection point, *i.e.,* virtual pivot point (Maus et al. 2010). ATRIAS has this capability to arbitrarily constrain leg forces, as demonstrated in Sections 4.2.3 and 4.2.4, and thus is amenable to virtual pivot techniques. Also, hybrid zero dynamics (HZD) has long offered various solutions to torso management which have been implemented on ATRIAS in-plane (Ramezani et al. 2013; Hereid et al. 2014).

Further, HZD formulations have been posited to formally collapse robot dynamics into a simpler spring-mass model using virtual constraints (Poulakakis and Grizzle 2009). With ATRIAS, such dynamics-matching techniques may be most applicable for two reasons. First, the passive dynamics already approximate a spring-mass model, likely requiring much less control effort to formally match the target model. Second, its impact-minimizing spring configuration is beneficial in satisfying hybrid invariance, a key control constraint for HZD methods. In effect, the discontinuous jump in state space is very small for the robot mass velocity and rotor velocity, which are normally quite sensitive variables for generating an invariant manifold.

While dynamic locomotion outside the sagittal plane remains an open controls challenge, several strategies already exist which can feasibly be implemented on ATRIAS. Despite traditional zero-moment point strategies being rendered moot by ATRIAS' point feet, strategically analogous push-recovery methods can be adapted to stabilize ATRIAS in three dimensions (Stephens and Atkeson 2010; Pratt et al. 2012). Hip abduction angles have been used to heuristically stabilize the

Raibert hoppers (Raibert 1986), and more formal abduction-control strategies have also been developed for the spring-mass model (Seipel and Holmes 2005; Peuker et al. 2012; Maus and Seyfarth 2014; Sullivan and Seipel 2014) and more have been developed in the context of HZD (Sinnet and Ames 2009; Hamed and Grizzle 2014; Buss et al. 2016). A strategy that works within the framework of spring-mass locomotion may help maximally leverage the machine's passive dynamics to achieve speed and efficiency. In fact, policies adapted from spring-mass studies, in combination with other components, are now exhibiting successful 3D locomotion with ATRIAS in simulation (Martin et al. 2015) and experiment (Rezazadeh et al. 2015).

5.3 Biological Investigation

Due the general similarities between spring-mass model and biological locomotion (Section 2), we can tune ATRIAS' parameters to more quantitatively match animal dynamics. Humans, birds, and other bipeds have long been characterized by an equivalent leg-spring stiffness, which ATRIAS can approximate by installing plate springs with stiffness to match.

In addition to effective stiffness, recent system identification work on ground-running birds from ostrich (120 kg) to quail (0.2 kg) has also estimated their effective leg dissipation (Birn-Jeffery et al. 2014). Reduced-order modeling of these species' running gaits suggested that the shape of their ground-reaction forces is consistent with work-optimal running control with actuated-spring-mass-damper legs, a math model highly similar to ATRIAS' legs. Specifically, the degree of dissipation in the reduced-order model was modulated to tightly fit to bird dynamical measurements, yielding an effective leg dissipation for each species' running gait. Interestingly, running ostriches (the species closest to ATRIAS in mass) exhibited a damping ratio of 0.058, which is notably similar to ATRIAS' damping ratio of 0.061. This suggests that ATRIAS can embody both the energy-cycling and energy-dissipating dynamics of animal gaits. Put more directly, ATRIAS may be very dynamically suited to run with ostrich-like gait dynamics.

This quantitative similarity to measured animal dynamics can be used to investigate animal running in a particularly comparable way. Specifically, if the underlying dynamics of ATRIAS are similar to animals, we hypothesize that energy-optimal control of ATRIAS should yield similar gaits to animals, which also likely minimize energy costs (Srinivasan and Ruina 2006). Tight correlations between optimal ATRIAS running and animal running would provide strong evidence for a more predictive reduced-order biological model. Such a model could be used to quantitatively predict animal maneuvers; a potentially important biological finding.

6 Conclusion

We present ATRIAS as an example of applying a spring-mass design approach to a versatile, human-scale bipedal robot. By leveraging a low-mass fourbar leg mechanism and series-elastic plate springs, ATRIAS exhibits spring-mass locomotion when dropped, pushed, or thrown. Thoughtfully actuating ATRIAS allows for both sustained walking and hopping on one leg (higher than humans), demonstrating a capability for executing a variety of gaits, and demonstrated preliminary walking with a specific cost of transport of 1.13 (approximately a third of energy cost estimates for ASIMO (Collins et al. 2005)). This versatility included hopping into, and out of, an unseen 16.5-cm-deep gravel pit, demonstrating notable control authority. Further, ATRIAS was able to step in place in 3D, untethered and unsupported, showing that ATRIAS is mechanically capable of locomotion in practical settings.

To our knowledge, ATRIAS is the first documented bipedal machine to replicate the human-like ground reaction forces of spring-mass walking. This characteristic "double-humped" force profile was measured both during a 17-step minimally controlled "passive" walk and a sustained steady walking (using a simple proof-of-concept walking controller). Further, the results also show hopping with the single-humped ground-reaction forces similar to animal running.

These biology-matching results advance a broader point regarding bioinspired robot design. Robot mechanisms need not be morphologically biomimetic (e.g. ATRIAS' spring-loaded fourbar leg mechanism) in order to produce biologically relevant dynamics (human ground-reaction forces). Further, these human-like dynamics emerge from efficient control of appropriately designed passive dynamics, and do not necessarily need to be the explicit target of a feedback control loop.

ATRIAS owes its dynamical capabilities to its

spring-mass design approach. The extent to which it performs varied motions are predicted by the simple model and the springs play a clear energetic role in the exhibited gaits. As such, these results embody an extension of theoretical compliant gait dynamics to more practical machines. Ultimately, the presented design and experiments demonstrate that insights from theoretical models are not limited to laboratory platforms, and in fact, can be a means for achieving the efficiency, versatility, and dynamism demanded of bipeds that the world will want.

Acknowledgments

This work was supported by the Defense Advanced Research Projects Agency [grant number W91CRB-11-1-0002]; the Human Frontier Science Program [grant number RGY0062/2010]; and the National Science Foundation [grant number CMMI-1100232].

The authors also thank their DARPA project collaborators: Dr. Jessy Grizzle and the Control Systems Laboratory at the University of Michigan, and Dr. Hartmut Geyer's research group at the Robotics Institute at Carnegie Mellon University. The authors also thank their HFSP project collaborator, Dr. Monica Daley of the Structure and Motion Laboratory at the Royal Veterinary College, London.

The authors further thank Kit Morton, Ryan Van Why, Soo-Hyun Yoo, Ethan Shepard, Michael Anderson, Ross McCullough, and Ryan Skeele for their technical contribution to building ATRIAS, its electronics and software systems, its supporting equipment, and their assistance in performing experiments.

References

[1] Andy Abate, Ross L. Hatton, and Jonathan Hurst. "Passive-dynamic leg design for agile robots". In: *2015 IEEE International Conference on Robotics and Automation (ICRA)*. 2015, pp. 4519–4524.

[2] Mojtaba Ahmadi and Martin Buehler. "The ARL Monopod II Running Robot: Control and Energetics". In: *IEEE Intl. Conf. on Robotics and Automation*. Detroit, May 1999, pp. 1689–1694.

[3] Richard Altendorfer, Ned Moore, Haldun Komsuoglu, Martin Buehler, H. Benjamin Brown Jr., Dave McMordie, Uluc Saranli, Robert J Full, and Daniel E. Koditschek. "RHex: a biologically inspired hexapod runner". In: *Autonomous Robots* 11 (2001), pp. 207–213.

[4] A. D. Ames. "Human-Inspired Control of Bipedal Walking Robots". In: *IEEE Transactions on Automatic Control* 59.5 (2014), pp. 1115–1130. ISSN: 0018-9286. DOI: 10.1109/TAC.2014.2299342.

[5] Emanuel Andrada, John Nyakatura, Roy Müller, Christian Rode, and Reinhard Blickhan. "Grounded Running: An Overlooked Strategy for Robots". In: *Autonomous Mobile Systems* (2012), pp. 79–87.

[6] Ben Andrews, Bruce Miller, John Schmitt, and Jonathan E. Clark. "Running over unknown rough terrain with a one-legged planar robot." In: *Bioinspiration & biomimetics* 6.2 (June 2011), p. 026009.

[7] Pranav A. Bhounsule, Jason Cortell, and Andy Ruina. "Design and control of Ranger: an energy-efficient, dynamic walking robot". In: *Proceedings of the Fifteenth International Conference on Climbing and Walking Robots and the Support Technologies for Mobile Machines (CLAWAR)*. 2012, pp. 441–448.

[8] Aleksandra Birn-Jeffery, Christian Hubicki, Yvonne Blum, Daniel Renjewski, Jonathan Hurst, and Monica Daley. "Don't break a leg: running birds from quail to ostrich prioritise leg safety and economy on uneven terrain". In: *Journal of Experimental Biology* 217.21 (2014), pp. 3786–3796.

[9] Reinhard Blickhan. "The Spring Mass Model for Running and Hopping". In: *Journal of Biomechanics* 22.11–12 (1989), pp. 1217–1227.

[10] Reinhard Blickhan and Robert J. Full. "Similarity in multilegged locomotion: bouncing like a monopode". In: *Journal of Comparative Physiology* 173.5 (1993), pp. 509–517.

[11] Yvonne Blum, Susanne W. Lipfert, Juergen Rummel, and André Seyfarth. "Swing leg control in human running". In: *Bioinspiration & biomimetics* 5.2 (June 2010), p. 026006.

[12] Thiago Boaventura, Claudio Semini, Jonas Buchli, Marco Frigerio, Michele Focchi, and Darwin G. Caldwell. "Dynamic torque control of a hydraulic quadruped robot". In: *Robotics and Automation (ICRA), 2012 IEEE International Conference on*. 2012, pp. 1889–1894.

[13] Brian G Buss, Kaveh Akbari Hamed, Brent A Griffin, and Jessy W Grizzle. "Experimental Results for 3D Bipedal Robot Walking Based On Systematic Optimization of Virtual Constraints". In: *American Control Conference* In review (2016).

[14] Katie Byl, Marten Byl, Martin Rutschmann, Brian Satzinger, Louis van Blarigan, Giulia Piovan, and Jason Cortell. "Series-elastic actuation prototype for rough terrain hopping". In: *2012 IEEE International Conference on Technologies for Practical Robot Applications (TePRA)*. Apr. 2012, pp. 103–110.

[15] Young-Hui Chang, Ronald A. Roiz, and Arick G. Auyang. "Intralimb compensation strategy depends on the nature of joint perturbation in human hopping." In: *Journal of biomechanics* 41.9 (Jan. 2008), pp. 1832–9.

[16] Baek-kyu Cho, Sang-sin Park, and Jun-ho Oh. "Stabilization of a hopping humanoid robot for a push". In: *2010 10th IEEE-RAS International Conference on Humanoid Robots* (Dec. 2010), pp. 60–65.

[17] Joseph S. Colett and Jonathan W. Hurst. "Artificial Restraint Systems for Walking and Running Robots: An Overview". In: *International Journal of Humanoid Robotics* 9.1 (2011).

[18] Steven H. Collins, Andy Ruina, Russ Tedrake, and Martijn Wisse. "Efficient bipedal robots based on passive-dynamic walkers". In: *Science* 307.5712 (2005), pp. 1082–1085.

[19] Monica A. Daley, James R. Usherwood, Gladys Felix, and Andrew A. Biewener. "Running over rough terrain; guinea fowl maintain dynamic stability despite a large unexpected change in substrate height". In: *Journal of Experimental Biology* 209.1 (2006), pp. 171–187.

[20] Georges Dalleau, Alain Belli, Muriel Bourdin, and Jean-René Lacour. "The spring-mass model and the energy cost of treadmill running." In: *European journal of applied physiology and occupational physiology* 77.3 (Feb. 1998), pp. 257–63.

[21] Tom Erez, Kendall Lowrey, Yuval Tassa, and Vikash Kumar. "An integrated system for real-time Model Predictive Control of humanoid robots". In: *IEEE/RAS International Conference on Humanoid Robots*. 2013.

[22] Michael Ernst, Hartmut Geyer, and Reinhard Blickhan. "Extension and customization of self-stability control in compliant legged systems." In: *Bioinspiration & biomimetics* 7.4 (Dec. 2012), p. 046002.

[23] Claire T. Farley, James Glasheen, and Thomas A. McMahon. "Running Springs: Speed and Animal Size". In: *Journal of Experimental Biology* 185.1 (Dec. 1993), pp. 71–86.

[24] Daniel P. Ferris, Mickey Louie, and Claire T. Farley. "Running in the real world: adjusting leg stiffness for different surfaces". In: *Proc. R. Soc. Lond. B Biol. Sci.* 265.1400 (Jan. 1998), pp. 989–993.

[25] Robert J. Full and Daniel E. Koditschek. "Templates and Anchors: Neuromechanical Hypotheses of Legged Locomotion on Land". In: *Journal of Experimental Biology* 202.23 (Dec. 1999), pp. 3325–3332.

[26] Robert J. Full, Timothy Kubow, John Schmitt, Philip Holmes, and Daniel Koditschek. "Quantifying Dynamic Stability and Maneuverability in Legged Locomotion". In: *Integrative and Comparative Biology* 42.1 (Feb. 2002), pp. 149–157.

[27] Hartmut Geyer, André Seyfarth, and Reinhard Blickhan. "Spring-mass running: simple approximate solution and application to gait stability". In: *Journal of theoretical biology* 232.3 (2005), pp. 315–328.

[28] Hartmut Geyer, Andrew Seyfarth, and Reinhard Blickhan. "Compliant leg behaviour explains basic dynamics of walking and running". In: *Proc. R. Soc. Lond. B.* 273.1603 (Nov. 2006), pp. 2861–2867.

[29] Raffaele M. Ghigliazza, Richard Altendorfer, Philip Holmes, and Daniel E. Koditschek. "A simply stabilized running model". In: *SIAM J. Applied. Dynamical Systems* 2.2 (2003), pp. 187–218.

[30] Jesse A. Grimes, Hamid Reza Vejdani, and Jonathan W. Hurst. "ATRIAS 1.0: Design and Demonstration of a Spring-Mass Hopping Robot in Human Scale". In: *Mechanism and Machine Theory, under review* (2014).

[31] Jessy W. Grizzle, Jonathan Hurst, Benjamin Morris, Hae Won Park, and Koushil Sreenath. "MABEL, A New Robotic Bipedal Walker and Runner". In: *American Control Conference*. St. Louis, Missouri, June 2009, pp. 2030–2036.

[32] Kaveh A. Hamed and Jessy W. Grizzle. "Event-based Stabilization of Periodic Orbits for Underactuated 3D Bipedal Robots with Left-Right Symmetry". In: *IEEE Transaction on Robotics* 30.2 (2014), pp. 365–381.

[33] Ayonga Hereid, Shishir Kolathaya, Mikhail S. Jones, Johnathan Van Why, Jonathan W. Hurst, and Aaron D. Ames. "Dynamic Multi-Domain Bipedal Walking with ATRIAS through SLIP based Human-Inspired Control". In: *Proceedings of the 17th international conference on Hybrid systems: computation and control*. 2014.

[34] Masato Hirose and Kenichi Ogawa. "Honda humanoid robots development." In: *Philosophical transactions. Series A, Mathematical, physical, and engineering sciences* 365.1850 (Jan. 2007), pp. 11–19.

[35] Daan Hobbelen, Tomas de Boer, and Martijn Wisse. "System overview of bipedal robots Flame and TUlip: Tailor-made for Limit Cycle Walking". In: *2008 IEEE/RSJ International Conference on Intelligent Robots and Systems*. Sept. 2008, pp. 2486–2491.

[36] Neville Hogan. "Impedance Control: An Approach to Manipulation: Part III - Applications". In: *Journal of dynamic systems, measurement, and control* 107.2 (1985), pp. 17–24.

[37] Christian M Hubicki and Jonathan W Hurst. "Running on soft ground: simple, energy-optimal disturbance rejection". In: *Proc 15th Int Conf on Climbing and Walking Robots (CLAWAR)*. 2012.

[38] Sang-Ho Hyon and Takashi Emura. "Symmetric walking control: Invariance and global stability". In: *IEEE/RSJ International Conference on Robotics and Automation (ICRA)*. April. 2005, pp. 1455–1462.

[39] Sang-Ho Hyon and Tsutomu Mita. "Development of a biologically inspired hopping robot-"Kenken"". In: *Robotics and Automation, 2002. Proceedings. ICRA '02. IEEE International Conference on*. Vol. 4. 2002, pp. 3984 – 3991.

[40] Kenji Kaneko, Fumio Kanehiro, Mitsuharu Morisawa, Kazuhiko Akachi, Go Miyamori, Atsushi Hayashi, and Noriyuki Kanehira. "Humanoid robot HRP-4-humanoid robotics platform with lightweight and slim body". In: *Intelligent Robots and Systems (IROS), 2011 IEEE/RSJ International Conference on*. 2011, pp. 4400–4407.

[41] Kevin Kemper, Devin Koepl, and Jonathan Hurst. "Optimal Passive Dynamics for Torque/Force Control". In: *International Conference on Robotics and Automation*. July 2010, pp. 2149–2154.

[42] Devin Koepl and Jonathan Hurst. "Impulse Control for Planar Spring-Mass Running". In: *Journal of Intelligent & Robotic Systems* 2 (Sept. 2013), pp. 1–15.

[43] David V. Lee, Michael R. Isaacs, Trevor E. Higgins, Andrew A. Biewener, and Craig P. McGowan. "Scaling of the Spring in the Leg during Bouncing Gaits of Mammals". In: *Integrative and comparative biology* 54.6 (2014), pp. 1099–1108.

[44] Susanne W. Lipfert, G Michael, Daniel Renjewski, Sten Grimmer, and Andre Seyfarth. "A model-experiment comparison of system dynamics for human walking and running". In: *Journal of Theoretical Biology* 292 (2012), pp. 11–17.

[45] Ian R. Manchester, Uwe Mettin, Fumiya Iida, and Russ Tedrake. "Stable dynamic walking over uneven terrain". In: *The International Journal of Robotics Research* 30.3 (Jan. 2011), pp. 265–279.

[46] William C Martin, Albert Wu, and Hartmut Geyer. "Robust Spring Mass Model Running for a Physical Bipedal Robot". In: *International Conference on Robotics and Automation* (2015), pp. 6307–6312.

[47] Horst-Moritz Maus and Andre Seyfarth. "Walking in circles: a modelling approach". In: *Journal of The Royal Society Interface* 11.99 (2014), p. 20140594.

[48] Moritz Maus, S W Lipfert, M Gross, J Rummel, and A Seyfarth. "Upright human gait did not provide a major mechanical challenge for our ancestors." In: *Nature communications* 1.6 (Jan. 2010), p. 70.

[49] Tad McGeer. "Passive dynamic walking". In: *International Journal of Robotics Research* 9.2 (1990), pp. 62–82.

[50] Ill-Woo Park, Jung-Yup Kim, Jungho Lee, and Jun-Ho Oh. "Mechanical design of the humanoid robot platform, HUBO". In: *Advanced Robotics* 21.11 (2007), pp. 1305–1322.

[51] Andrew Peekema, Daniel Renjewski, and Jonathan W. Hurst. "Open-Source Real-Time Robot Operation and Control System for Highly Dynamic, Modular Machines". In: *ASME International Design Engineering Technical (IDET)*. 2013.

[52] Frank Peuker, Christophe Maufroy, and André Seyfarth. "Leg-adjustment strategies for stable running in three dimensions." In: *Bioinspiration & biomimetics* 7.3 (Sept. 2012), p. 036002.

[53] Giulia Piovan and Katie Byl. "Two-element control for the active SLIP model". In: *2013 IEEE International Conference on Robotics and Automation* (May 2013), pp. 5656–5662.

[54] Ioannis Poulakakis and Jessy W. Grizzle. "The Spring Loaded Inverted Pendulum as the Hybrid Zero Dynamics of an Asymmetric Hopper". In: *IEEE Transactions on Automatic Control* 54.8 (Aug. 2009), pp. 1779–1793.

[55] J. Pratt, T. Koolen, T. de Boer, J. Rebula, S. Cotton, J. Carff, M. Johnson, and P. Neuhaus. "Capturability-based analysis and control of legged locomotion, Part 2: Application to M2V2, a lower-body humanoid". In: *The International Journal of Robotics Research* 31.10 (Aug. 2012), pp. 1117–1133.

[56] Jerry Pratt, Chee-Meng Chew, Ann Torres, Peter Dilworth, Gill Pratt, and M C Chee. "Virtual model control: an intuitive approach for bipedal locomotion". In: *The International Journal of Robotics Research* 20.2 (2001), pp. 129–143.

[57] Marc H. Raibert. *Legged robots that balance*. Vol. 29. 6. Mass.: MIT Press, 1986, pp. 499–514.

[58] Alireza Ramezani, Jonathan W. Hurst, Kaveh Akbari Hamed, and Jessy W. Grizzle. "Performance Analysis and Feedback Control of ATRIAS, A 3D Bipedal Robot". In: *Journal of Dynamic Systems, Measurement, and Control* 136.2 (2013), p. 021012.

[59] Daniel Renjewski. "An Engineering Contribution to Human Gait Biomechanics". PhD Dissertation. TU Ilmenau, 2012.

[60] Siavash Rezazadeh, Christian M. Hubicki, Mikhail Jones, Andrew Peekema, Johnathan Van Why, Andy Abate, and Jonathan Hurst. "Spring-mass Walking with ATRIAS in 3D: Robust Gait Control Spanning Zero to 4.3 KPH on a Heavily Underactuated Bipedal Robot". In: *Proceedings of the ASME 2015 Dynamic Systems and Control Conference ASME/DSCC 2015*. 2015.

[61] David W Robinson, Jerry E Pratt, Daniel J Paluska, and Gill A Pratt. "Series Elastic Actuator Development for a Biomimetic Walking Robot". In: *IEEE/ASME international conference on advanced intelligent mechatronics*. Sept. 1999, pp. 561–568.

[62] Fredrik Roos, Hans Johansson, and Jan Wikander. "Optimal selection of motor and gearhead in mechatronic applications". In: *Mechatronics* 16.1 (Feb. 2006), pp. 63–72.

[63] Justin E. Seipel and Philip Holmes. "Running in Three Dimensions: Analysis of a Point-mass Sprung-leg model". In: *International Journal of Robotics Research* 24.8 (Aug. 2005), pp. 657–674.

[64] Sangok Seok, Albert Wang, David Otten, Jeffrey Lang, and Sangbae Kim. "Design principles for highly efficient quadrupeds and implementation on the MIT Cheetah robot". In: *2013 IEEE International Conference on Robotics and Automation* (May 2013), pp. 3307–3312.

[65] Andre Seyfarth and Hartmut Geyer. "Natural Control of Spring-Like Running: Optimised Self-Stabilisation". In: *International Conference on Climbing and Walking Robots*. 1. 2002, pp. 81–85.

[66] Andre Seyfarth, Hartmut Geyer, and Hugh M. Herr. "Swing-leg retraction: a simple control model for stable running". In: *The Journal of Experimental Biology* 206.15 (Aug. 2003), pp. 2547–2555.

[67] Ryan W Sinnet and Aaron D Ames. "3D bipedal walking with knees and feet: A hybrid geometric approach". In: *Decision and Control, 2009 held jointly with the 2009 28th Chinese Control Conference. CDC/CCC 2009. Proceedings of the 48th IEEE Conference on*. IEEE. 2009, pp. 3208–3213.

[68] Mark Spong. "Underactuated mechanical systems". In: *Control Problems in Robotics and Automation*. Ed. by Bruno Siciliano and Kimon Valavanis. Vol. 230. Lecture Notes in Control and Information Sciences. Springer Berlin / Heidelberg, 1998, pp. 135–150.

[69] Alexander Spröwitz, Alexandre Tuleu, Massimo Vespignani, Mostafa Ajallooeian, Emilie Badri, and Auke Jan Ijspeert. "Towards Dynamic Trot Gait Locomotion: Design, Control, and Experiments with Cheetah-cub, a Compliant Quadruped Robot". In: *The International Journal of Robotics Research* 32.8 (2013), pp. 932–950.

[70] Koushil Sreenath, Hae Won Park, Ioannis Poulakakis, and Jessy W. Grizzle. "Embedding active force control within the compliant hybrid zero dynamics to achieve stable, fast running on MABEL". In: *The International Journal of Robotics Research* 32.3 (Mar. 2013), pp. 324–345.

[71] Manoj Srinivasan and Andy Ruina. "Computer optimization of a minimal biped model discovers walking and running". In: *Nature* 439.7072 (Jan. 2006), pp. 72–75.

[72] Benjamin J. Stephens and Chris G. Atkeson. "Dynamic Balance Force Control for compliant humanoid robots". In: *2010 IEEE/RSJ International Conference on Intelligent Robots and Systems* (Oct. 2010), pp. 1248–1255.

[73] Timothy Sullivan and Justin Seipel. "3D dynamics of bipedal running: Effects of step width on an amputee-inspired robot". In: *IEEE International Conference on Intelligent Robots and Systems*. 2014, pp. 939–944. ISBN: 9781479969340. DOI: 10.1109/IROS.2014.6942672.

[74] Junichi Urata, Yuto Nakanishi, Kei Okada, and Masayuki Inaba. "Design of high torque and high speed leg module for high power humanoid". In: *2010 IEEE/RSJ International Conference on Intelligent Robots and Systems* (Oct. 2010), pp. 4497–4502.

[75] Miomir Vukobratović and Branislav Borovac. "Zero-Moment Point–Thirty Five Years of its Life". In: *Intl. J. of Humanoid Robotics* 1.1 (2004), pp. 157–173.

[76] K. J. Waldron and G. L. Kinzel. "The relationship between actuator geometry and mechanical efficiency in robots". In: *Fourth Symposium on Theory and Practice of Robots and Manipulators*. 1981.

[77] Eric R. Westervelt, Jessy W. Grizzle, and Daniel E. Koditschek. "Hybrid Zero Dynamics of Planar Biped Walkers". In: *IEEE Transactions on Automatic Control* 48.1 (Jan. 2003), pp. 42–56.

[78] Garth Zeglin. "The Bow Leg Hopping Robot". PhD thesis. Pittsburgh, PA: Robotics Institute, Carnegie Mellon University, Oct. 1999.

[79] Tingnan Zhang, Feifei Qian, Chen Li, Pierangelo Masarati, Aaron M. Hoover, Paul Birkmeyer, Andrew Pullin, Ronald S. Fearing, and Daniel I. Goldman. "Ground fluidization promotes rapid running of a lightweight robot". In: *The International Journal of Robotics Research* 32.7 (July 2013), pp. 859–869.

A Power Analysis

Using a preliminary example gait controller (as per Section 4.3.2), we were able to identify ATRIAS' typical, main *actuator power profile*. ATRIAS' load scenario is given through its four main actuator velocities, their in-series spring/actuator torques, and the measured power. This was particularly important for assessing the empirical effect of the leg mechanism's geometric power on the electrical economy on a walking gait (See Section 3.3.1 and its associated power data, Figure 8). Observing a walking gait with a speed of 0.85 m/s, the mean data of 12 consecutive steps were recorded and analyzed.

A motor model was implemented to fill gaps from non-measurable, otherwise missing dynamical motor characteristics (See Table A.1 for a list of available sensors). Power "components," such as ratio of regeneration, electrical power losses, and individual motor powers were non-measurable, mostly because they were not accessible in the ATRIAS setup. Only the instantaneous summed power of all four actuators could be measured by a power clamp. Consequently, we present an ATRIAS motor model that provides otherwise unaccessible system parameters such as *a*) instantaneous power applied to accelerate actuators, *b*) electrical power losses, *c*) actuator efficiencies, *d*) and the instantaneous regeneration of actuators and amplifiers. The model further allows for precise estimation of the swing and stance phase power characteristics of the ATRIAS system given the example gait controller.

A.1 Experimental Setup

Full dynamics in a legged robotic system can be derived if both kinematic and dynamic data are available. ATRIAS' sensor infrastructure provides sufficient information to calculate the instantaneous load on each actuator continuously during the swing and stance phases. Axial leg forces and tangential leg torques were measured indirectly through the robot's deflecting leg springs, one for each of ATRIAS leg motors (Section 3.2.2). Leg forces and torques are derived through the robot's kinematics and the measured actuator forces and torques. In a system without internal actuator torque estimation, swing phase dynamics cannot be estimated. Few robots are equipped with a full set of joint torque sensors, and only sparse data of robot swing phase dynamics is available from literature. ATRIAS's internal leg dynamic measurements directly enable us to measure those values and apply them in the motor model to gain insights into details of the system's motor power.

All sensor data was recorded at a sampling frequency of 1000 Hz. The data of the walking ATRIAS robot was recorded over 12 full locomotion cycles. A full cycle was arbitrarily defined between the beginning of the left leg swing phase, and the end of the left leg stance phase. The average gait cycle time was 1.1sec, at a gait cycle duty factor of 0.6 (Figure 18, stance duration per gait cycle). The motor-torque crossing from loaded to unloaded, of the left leg motor-B, was used to define the onset of swing phase, and the end of stance phase again. All cycles were cut manually, and trajectories were interpolated with 1000 samples.

A.2 Motor Model

We implemented a variant of the motor model by (Roos et al. 2006), for each of ATRIAS' four main actuators. Only the sum of the applied current for all four motors (ABAB) could be measured in the ATRIAS setup, with the help of a single current clamp (P_{clamp}). The load-motor model allowed us to approximate the individual, instantaneous current of each motor. Further, we extended Roos' motor model with the capability of identifying actuators in generator mode; in phases of negative power, those actuators would push electrical power back into the robot's electrical grid. We found that this regenerated power was almost always instantly re-used by one of the other motors, and did not charge the batteries. This a consequence of the geometric power inherent to the mechanism as described in Section 3.3.1.

Motor power P_m is described as the sum of electrical losses P_elec and mechanical losses P_mech (Roos et al. 2006, equation 10-13) for a system without power regeneration of mechanical energy. Mechanical losses depend on the instantaneous power applied through the load (T_l, $\dot{\theta}_\mathrm{l}$) and through accelerating the motor and gear components (J_m motor inertia, J_g gearbox inertia).

$$P_\mathrm{m} = P_\mathrm{elec} + P_\mathrm{mech} \quad (1)$$

$$P_\mathrm{mech} = (J_\mathrm{m} + J_\mathrm{g})\ddot{\theta}_\mathrm{l}\dot{\theta}_\mathrm{l}n^2 + \frac{T_\mathrm{l}}{\mu_\mathrm{g}}\dot{\theta}_\mathrm{l} \quad (2)$$

$$P_\mathrm{elec} = R_\mathrm{m}I^2 = R_\mathrm{m}\frac{T_\mathrm{m}^2}{k_\mathrm{T}^2} \quad (3)$$

θ_l indicates the position of the load, here the actuator position in [rad], $\dot{\theta}_\mathrm{l}$ its velocity and $\ddot{\theta}_\mathrm{l}$ its acceleration. T_l in [Nm] is the load torque measured through spring deflection, $\mu_{\mathrm{g}\,(50\%)}$ is the approximation of the harmonic drive gearbox efficiency. Electrical losses are calculated through the motor winding resistance (R_m in [Ω]), and the motor coefficient k_T. n is the gear ratio of the harmonic drive. We externally measured ATRIAS' electrical power P_clamp and compared it to the model-predicted motor power $P_\mathrm{m,robot}$, as sum of its four main leg actuators [motor ID's: (L) left and (R) right side, A and B motor]:

$$P_\mathrm{m,robot} = P_\mathrm{m,LA} + P_\mathrm{m,LB} + P_\mathrm{m,RA} + P_\mathrm{m,RB} \quad (4)$$

Measured State	Type of Sensor	Source	Model Number
Motor rotor (transmissive encoder)	3,500 Lines/Rev. Incremental Quadrature	US Digital	3500-EM1-0-360-I
Motor rotor (hall effect)	3 sensors (1 per phase)	Emoteq	
Motor winding thermistor	temperature	Digikey	
Spring + Limb Angles	1nm Absolute Optical w/ RTLA-S martensitic steel scale (294μRad/bit)	Renishaw	RL32BAT001B30F
Leg Abduction	13-bit Absolute Magnetic Encoder	Renishaw	RMB30SI13BC1
Ground Contact	Custom Full-Bridge Load Cell	Omega	120 Ohm Linear Foil Gauge
Knee Sideload	Custom Quarter-Bridge Load Cell	' '	' '
R.O.M. Limits	SPDT NC	Omron	D2F-01FL-D
Robot pitch (via Boom)	17-bit absolute (geared to 12.6μRad/bit)	Hengstler	AC36/0017AR.41SBB
Robot horizontal (via Boom)	17-bit absolute (geared to 107.3μm/bit)	' '	' '
Robot vertical (via Boom)	17-bit absolute (geared to 26.8μm/bit)	' '	' '

Table 1: Detailed list of sensors to measure state information on ATRIAS.

The above motor model, however, does not account for the imperfect generator mode of the actuators and power amplifier in the case of negatively applied power. Only externally applied loads, or load through acceleration can produce negative power (equation 2). We include a generator efficiency term μ_{regen} into the equation for the motor power P_m:

$$P_{\text{mech,regen,motorID}} = -\mu_{\text{regen}} P_{\text{mech,motorID}} \quad (5)$$

$$P_m = P_{elec} + P_{mech} + P_{mech,regen} \quad (6)$$

and we identified the efficiency of regeneration between $\mu_{\text{regen}} = 30\,\%$ and $40\,\%$.

A.3 Power Analysis Results

The average, minimal and maximal leg forces and leg torques per full gait cycle of this example gait are given in Figure 18 (top and bottom, respectively). The leg force profile shows the walking-gaits-specific double hump profile, with a maximum leg force of 650 N. Leg torques reached from -130 Nm up to 100 Nm, and showed much higher variations, compared to the robot's leg forces (Figure 18).

Quantitative results from the ATRIAS motor model are presented in Table A.3, separated by stance phase values (40 % of cycle time), swing phase values, and full cycle values (1.1 sec in average). The motor model is based on individual sensor data of the left and right ATRIAS leg, and indicates that both legs are not working in complete symmetry. Because the robot is walking in a circle, forces and torques applied are different between its inner (left) and outer (right) leg. Here shown are only motor model power values for the left robot leg. Power values are provided, hence the mean of stance and swing, weighted by the duty factor, gives the full cycle power values. The externally applied load ($P_{\text{l,A}}$ and $P_{\text{l,B}}$) during stance phase is caused by impact and weight of the robot, and during swing phase by the mass and inertia of the legs ($P_{\text{l,AB,swing}} \approx 15\,\text{W}$). Swing power values are very low, due to the low-weight leg design of ATRIAS. During stance phase motor-A shows a large positive power consumption $P_{\text{l,A,stance}} = 273\,\text{W}$, as it is supporting the weight of the robot. Motor-B is showing an almost equally large, but negative power, because the direction of torque is opposite to that of motor A (four-bar construction), while the direction of movement is identical (backwards). Parts of this negative power are being pushed back through the amplifiers, into other, power-draining motors ($P_{\text{regen,B,stance}} = -57\,\text{W}$). As a consequence of a large stance phase torque at lower motor speed, the electrical power losses of motor-A are significant: $P_{\text{elec,A,stance}} = 99\,\text{W}$, or almost 1/3 of the load power.

Mechanical swing phase power (instantaneous sum of load and acceleration) is roughly equal between motor-A and motor-B actuators. Though leg masses

Type	Motor	Side	Swing	Stance	Full
P_{m}	A	L	135	363	265
P_{m}	B	L	119	-57	19
P_{m}	ABAB	LR	584	517	546
P_{mech}	A	L	151	265	216
P_{mech}	B	L	157	0	67
P_{mech}	ABAB	L	606	510	551
P_{l}	A	L	14	273	162
P_{l}	B	L	16	-268	-146
P_{l}	ABAB	LR	19	22	21
P_{acc}	A	L	12	-9	0
P_{acc}	B	L	-31	25	1
P_{acc}	ABAB	LR	-24	20	1
P_{elec}	A	L	20	99	65
P_{elec}	B	L	13	0	6
P_{elec}	ABAB	LR	137	128	132
P_{regen}	A	L	-36	0	-15
P_{regen}	B	L	-51	-57	-55
P_{regen}	ABAB	LR	-159	-121	-137
P_{clamp}	ABAB	LR	559	573	567

Table 2: P_{m} indicates the cummulative, modeled motor power (Equation 1), P_{mech} the modeled, instantaneous sum of the external load power P_{l} and the internal load power P_{acc} (both with positive and negative values). Latter is caused by the acceleration of motor and gearbox components. Swing time of this gait covers approximatively 40 %. The externally measured power over all four motors (ABAB), is shown as $P_{clamp(ABAB)}$. All values are reported in [W].

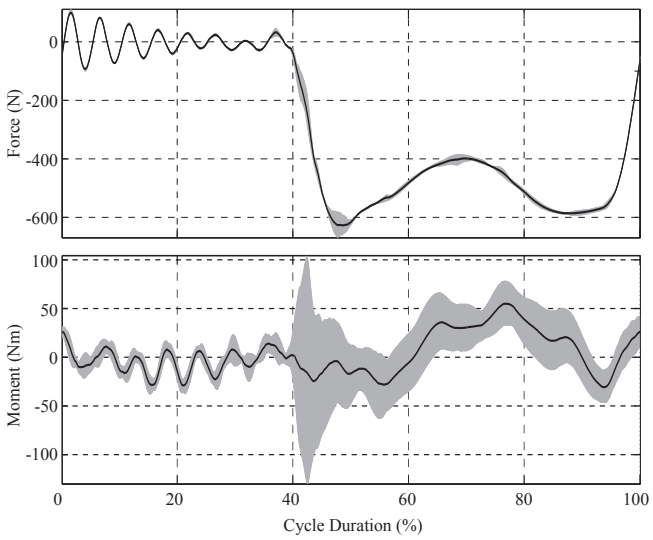

Figure 18: ATRIAS' leg forces (top) and leg torques (bottom), x-values are normalized by a full gait cycle of a walking gait with an average forward speed of 0.85 m/s. Values of the left leg only are shown. The plot starts with the swing phase, stance phase begins at 40 % of the gait cycle. Continues, bold lines show average force and torque values over 12 strides, grey shaded areas indicate the maximum and minimum band. Maximum leg forces during the walking experiment were around 650 N. Stance phase of the leg torques indicates an initial braking phase (average −25 Nm), followed by a longer pushing phase (average 55 Nm), and a final, short braking torque burst (−30 Nm). Strong oscillations of the leg in swing phase are visible both as leg forces, and as leg torque during the first 40 % of the gait cycle.

are low, both actuators require larger accelerations during swing phase, which is 20 % shorter than the robot's stance phase. Further, leg length is shortened in addition to the swing-forward movement, which adds an additional acceleration component to the actuators. For the full cycle and both legs, the motor model predicts an electrical power consumption of $P_{\mathrm{m}} = 546\,\mathrm{W}$, versus a measured power consumption of $P_{\mathrm{clamp}} = 567\,\mathrm{W}$. For the ATRIAS system, this corresponds to an electrical cost of transport of 1.13 for this preliminary example gait.

B Comparative Hopping Analysis

While one-legged hopping is a common diagnostic test for various human medical conditions, the center-of-mass hopping height is rarely measured and reported in human studies. We estimate one-legged hopping height in humans using more commonly reported measurements, which we analyze using work-energy methods. Specifically, we infer center-of-mass hopping height using subject mass (m), peak force measurements (F_{pk}) and center-of-mass compression while on the ground (h_c). We used measurements of these quantities from (Chang et al. 2008), which included an experimental control group which hopped on one foot at a "comfortable" 2.2 Hz human hopping tempo.

We begin by defining work-energy equations at the highest position of the center of mass (apex), and the lowest point while the ground (zenith).

$$E_{apex} = E_{zenith} + W_{nonconserved} \qquad (7)$$

At both apex and zenith, the center-of-mass velocity is zero, reducing the energy terms to the difference in gravitational potential. Further, since the force-length relation of human hopping was highly linear ($r^2 = 0.99$ and visible in (Chang et al. 2008, Figure 3a)), we can accurately approximate the leg work as the area under the force-length curve, which is a triangle:

$$mg\left(h_{hop} + h_c\right) = \frac{1}{2} F_{pk} h_c \quad (8)$$

where h_{hop} is the desired quantity, the vertical distance the center of mass travels after take off. Given quantities are: m, the subject mass, g, gravitational acceleration, F_{pk}, the peak leg force, and h_c, the distance the leg compresses during stance. This equation simplifies to:

$$h_{hop} = \left(\frac{F_{pk}}{2mg} - 1\right) h_c \quad (9)$$

where (Chang et al. 2008, Table 1)) gives m=59.1±9.2 kg (very close to ATRIAS' 62 kg with batteries), g=9.81 m/s^2, F_{pk}=1570±207 N, and h_c=8.18±0.36 cm.

Further, we employ an error propagation analysis on peak force and leg compression (the parameters that change from hop to hop) given their reported standard deviations. We derive a standard deviation for h_{hop}, $\sigma_{h_{hop}}$ as:

$$\sigma_{h_{hop}} = \sqrt{\left(\frac{\delta h_{hop}}{\delta F_{pk}}\right)^2 \sigma^2_{F_{pk}} + \left(\frac{\delta h_{hop}}{\delta h_c}\right)^2 \sigma^2_{h_c}} \quad (10)$$

$$\sigma_{h_{hop}} = \sqrt{\left(\frac{h_c}{2mg}\right)^2 \sigma^2_{F_{pk}} + \left(\frac{F_{pk}}{2mg} - 1\right)^2 \sigma^2_{h_c}} \quad (11)$$

which evaluates to h_{hop}=2.9±1.5 cm, significantly lower than ATRIAS' hopping height of 9.6±0.9 cm. In the main text (Section 4.3.1), we report the high end of this computed range, which is 4.4 cm. Further, we can employ a maximally generous statistical interpretation and assume the best-case values within the human statistical range (high leg compression, 8.54 cm, high peak force, 1777 kg, and low mass, 49.9 kg), and compute a human hopping height of 7.0 cm, which is also eclipsed by ATRIAS.

We believe that our presented center-of-mass measurements demonstrate ATRIAS' capability for sustainable one-legged hopping on par with human capability. We believe this is the first documentation of sustainable human-level hopping performance with a human-scale biped that can operate off-tether. While other tether-free-capable humanoid robots can hop (Cho et al. 2010), and ASIMO can hop on one leg, it is difficult to estimate exactly how far the center of mass is vaulted from presented data. Further, the high-powered HRP3L-JSK (Urata et al. 2010) has been shown to jump a very-significant 44 cm off the ground. This HRP3L-JSK test attempts a single hop using both legs, does not attempt a safe landing, and rapidly retracts its legs during flight, thereby reporting a hopping height that differs from the height of the center of mass.

C Control for Experiments

The ATRIAS validation controllers are designed to regulate quantities in the axial and rotational directions in the plane. The purpose of these proof-of-concept controllers is to embody the dynamical properties of the spring-mass model. For instance, the passive spring mass model has a fixed rest length of the spring and no net torques about the center of mass. On ATRIAS, these properties can be implemented as targets of control.

First, we define our coordinate system as per Figure 19. The planar ATRIAS has four motor angles ($\theta_m = [\theta_{1sm}, \theta_{2sm}, \theta_{1nsm}, \theta_{2nsm}]^T$) as depicted in Figure. The robot also has access to the angles of the leg linkages, which are on the distal side of the spring ($\theta_l = [\theta_{1sl}, \theta_{2sl}, \theta_{1nsl}, \theta_{2nsl}]^T$). Using these angles, we can construct functions for all of our key quantities we wish to regulate, including leg angles, leg force, and hip torque.

For our general controller, we define a simple PD control law that regulates the position of each motor angle

$$\tau = K_P\left(\theta_m^{des} - \theta_m\right) - K_D\dot{\theta}_m \quad (12)$$

where $\tau = [\tau_{1s}, \tau_{2s}, \tau_{1ns}, \tau_{2ns}]$ are commanded motor torques to their matching motor angles (θ_m) and K_P and K_D are proportional and derivative gains respectively. $\theta_m^{des} = \left[\theta_{1sm}^{des}, \theta_{2sm}^{des}, \theta_{1nsm}^{des}, \theta_{2nsm}^{des}\right]^T$ are the desired position of the motor angles and are determined differently for each experiment. In general form, θ_m^{des} is the solution to the system of equations:

$$g^s_{axial}(\theta_m^{des}, \theta_l) = y^s_{axial}$$

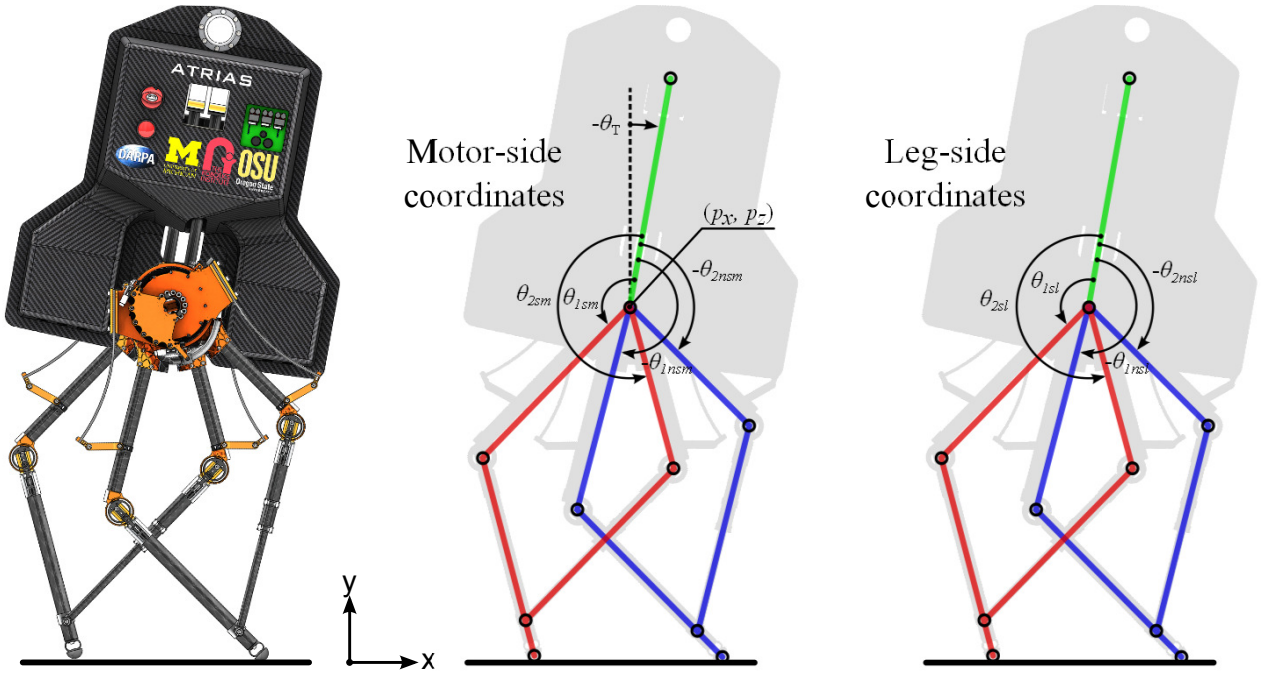

Figure 19: Coordinate system for the ATRIAS bipedal robot in the sagittal plane. The middle drawing points to angles of the motors and the rightmost illustration points to angles of the deflected springs.

$$\begin{aligned} g^s_{rot}(\theta^{des}_m, \theta_l) &= y^s_{rot} \\ g^{ns}_{axial}(\theta^{des}_m, \theta_l) &= y^{ns}_{axial} \\ g^{ns}_{rot}(\theta^{des}_m, \theta_l) &= y^{ns}_{rot} \end{aligned}$$

at any given instant, where $g(\theta^{des}_m, \theta_l) = [g^s_{axial}, g^s_{rot}, g^{ns}_{axial}, g^{ns}_{rot}]$ are functions defining our key regulated quantities and $y = [y^s_{axial}, y^s_{rot}, y^{ns}_{axial}, y^{ns}_{rot}]$ defines the target value of the quantity. The subscripts *axial* and *rot* indicate axial and rotational quantities and the superscripts s and ns denote the stance and nonstance legs respectively. These functions are defined below and apportioned to each experiment in Table 3.

We now define our key quantities to be used in the experiments. The rest length of the virtual spring is solely a function of motor positions, θ_m. The deflections of each rotational spring can be calculated from the difference between motor and leg angles $(\theta_m - \theta_l)$. We use this information to compute the zero-force length of the leg mechanism measured from the hip position (p_x, p_z) via:

$$l^s_0(\theta_m) = L_{sh}\cos(\theta_{1sm}) + L_{th}\cos(\theta_{2sm}) \quad (13)$$

$$l^{ns}_0(\theta_m) = L_{sh}\cos(\theta_{1nsm}) + L_{th}\cos(\theta_{2nsm}) \quad (14)$$

where l^s_0 and l^{ns}_0 are the zero force leg lengths of the stance and non-stance legs respectively, and the lengths of the thigh and shin (L_{th} and L_{sh}) are both $0.5m$. We further require the deflected length of the virtual spring (l^s_k) to compute axial forces:

$$l^s_k(\theta_m) = L_{sh}\cos(\theta_{1sl}) + L_{th}\cos(\theta_{2sl}) \quad (15)$$

$$F^s = k_s \frac{\sqrt{1-l^{s\,2}_k} - (\arccos l^s_k - \arccos l^s_0)\, l_k}{2L_{sh}L_{th}\sqrt[3]{1-l^{s\,2}_k}}\,(l^s_k - l^s_0) \quad (16)$$

where F^s (a function of l^s_k and l^s_0) is the force in the axial direction of the leg when given a rotational spring stiffness of the plate springs (k_s). Rotational zero-force leg angles and deflected angles reduce to mere averages of the mechanism's angles:

$$\theta^s_0(\theta_m) = \frac{1}{2}(\theta_{1sm} + \theta_{2sm}) \quad (17)$$

$$\theta^{ns}_0(\theta_m) = \frac{1}{2}(\theta_{1nsm} + \theta_{2nsm}) \quad (18)$$

$$\theta^s_k(\theta_l) = \frac{1}{2}(\theta_{1sl} + \theta_{2sl}) \quad (19)$$

$$\theta^{ns}_k(\theta_l) = \frac{1}{2}(\theta_{1nsl} + \theta_{2nsl}) \quad (20)$$

where θ^s_0 and θ^{ns}_0 are the zero-force leg angles and θ^s_k and θ^{ns}_k are the deflected leg angles for the stance and non-stance legs respectively. This allows us to

Experiment	Phase	Axial ($g_{axial} \rightarrow y_{axial}$)	Rotational ($g_{rot} \rightarrow y_{rot}$)
#1 Passive Drop	N/A	N/A	N/A
#2 Passive Walking	Stance Leg	Constant Rest Length ($l_0^s \rightarrow 0.9m$)	Zero-torque ($\delta_k^s \rightarrow 0$)
	Non-stance	Rest-length trajectory ($l_0^{ns} \rightarrow l(\alpha)$)	Angle ($\theta_0^{ns} \rightarrow \theta(\alpha)$)
#3 Passive Throw	Stance	Constant Rest Length ($l_0^s \rightarrow 0.9m$)	Zero-torque ($\delta_k^s \rightarrow 0$)
	Flight	Nominal rest length ($l_0^s \rightarrow 0.9m$)	Leg angle ($\theta_0^s \rightarrow \theta_{TD}$)
#4 Hopping	Stance	Regulate force profile ($F^s \rightarrow f(t)$)	Hold vertical ($\theta_0^s \rightarrow \pi$)
	Flight	Nominal rest length ($l_0^s \rightarrow 0.9m$)	Hold vertical ($\theta_0^s \rightarrow \pi$)
#5 Sustained Walking	Stance Leg	Constant Rest Length ($l_0^s \rightarrow 0.9m$)	Small torque ($\delta_k^s \rightarrow \epsilon$)
	Non-stance	Rest length trajectory ($l_0^{ns} \rightarrow l(\alpha)$)	Angle traj. ($\theta_0^{ns} \rightarrow \theta(\alpha)$)
#6 Hops in Rocks	Stance	Regulate force profile ($F^s \rightarrow f(t)$)	Hold vertical ($\theta_0^s \rightarrow \pi$)
	Flight	Nominal rest length ($l_0^s \rightarrow 0.9m$)	Hold vertical ($\theta_0^s \rightarrow \pi$)
#7 Balancing in 3D			(Rezazadeh et al. 2015)

Table 3: A comparative summary of the controllers used for the ATRIAS validation experiments. Each leg has two motors, and thus has two target quantities for the controller to regulate at all times (one in the axial direction and one in the rotational direction). These quantities are driven via PD controllers to the value indicate by the $\rightarrow$ symbol. ϵ is a small torque offset, α is the angle of the stance leg with respect to vertical, θ_{TD} is an angle determined by simulations with the spring-mass model, and $f(t)$ is a time-dependent force trajectory derived from numerical simulations of the spring-mass model.

compute the deflection of the mechanisms' virtual rotational spring

$$\delta_k^s(\theta_m, \theta_l) = \theta_0^s - \theta_k^s \quad (21)$$
$$\delta_k^{ns}(\theta_m, \theta_l) = \theta_0^{ns} - \theta_k^{ns} \quad (22)$$

where δ_k^s and δ_k^{ns} are the rotational spring deflections for the stance and non-stance legs respectively.

Example. Let's take the example of the passive walking test (Section 4.2.3 and Experiment #2 in Table 3). For the stance leg, the axial target is a constant rest length (l_0^s) of $0.9m$ and the rotational target is a leg torque (δ_k^s) of zero. For the non-stance leg, the axial target is a nonstance leg length (l_0^{ns}) that is a function of the stance leg angle, α, which is designed to lift and lower the leg through swing. The nonstance rotational target is nonstance leg angle, which that too varies with α, which in this case is designed to swing the leg forward as α increases. We then solve for the set of four desired motor angles θ_m^{des} which satisfies all four of these conditions:

$$\begin{aligned} l_0^s(\theta_m^{des}, \theta_l) &= L_{sh}\cos\left(\theta_{1sm}^{des}\right) + L_{th}\cos\left(\theta_{2sm}^{des}\right) \\ &= 0.9m \\ \delta_k^s(\theta_m^{des}, \theta_l) &= \theta_0^s - \theta_k^s \\ &= \frac{1}{2}\left(\theta_{1sm}^{des} + \theta_{2sm}^{des}\right) - \frac{1}{2}(\theta_{1sl} + \theta_{2sl}) \\ &= 0 \\ l_0^s(\theta_m^{des}, \theta_l) &= L_{sh}\cos\left(\theta_{1nsm}^{des}\right) + L_{th}\cos\left(\theta_{2nsm}^{des}\right) \\ &= l(\alpha) \\ \theta_0^{ns}(\theta_m^{des}, \theta_l) &= \frac{1}{2}\left(\theta_{1nsm}^{des} + \theta_{2nsm}^{des}\right) \\ &= \theta(\alpha). \end{aligned}$$

These conditions fully describe, for that instant, all four target motor angles, θ_{1sm}^{des}, θ_{2sm}^{des}, θ_{1nsm}^{des}, and θ_{2nsm}^{des}. These θ_m^{des} are then fed to the controller (12) to compute commanded motor torques, τ.

Extension	Type	Description
1	Video	a) Figure 10 test (0:06)
		b) Figure 11 test (0:17)
		c) Figure 13 test (0:43)
		d) Figure 14 test (0:52)
		e) Figure 15 test (1:01)
		f) Figure 16 test (1:19)
		g) Figure 17 test (2:06)

Table 4: List of multimedia extensions.